UNIVERSITY OF CALIFORNIA
RIVERSIDE

Performance Limits of Outdoor Wireless Optical Communication Links through Scattering and Turbulent Channels

A Dissertation submitted in partial satisfaction
of the requirements for the degree of

Doctor of Philosophy

in

Electrical Engineering

by

Qunfeng He

September 2012

Dissertation Committee:

Professor Zhengyuan Xu , Chairperson
Professor Ertem Tuncel
Professor Jianlin Liu

The Dissertation of Qunfeng He is approved:

Committee Chairperson

University of California, Riverside

Acknowledgments

It was five years ago when I received a long distance phone call from Prof. Zhengyuan Xu talking about the opportunity to join his group. Since then, my life changed enormously in a way I feel so much excited with. To me, Prof. Xu is like a mentor, a friend and moreover, a model in his way of exploring the unknown academic fields. Five years later, as I'm about to commence, I owe so much heartily-felt gratitude to Prof. Xu for allowing me to savor the pleasure of research in discovering, understanding and solving the real world problems. It's something more than the courses, books and papers. It's the enthusiasm to chase the challenging but intriguing topics, which inspires me all along these years' journey and it will continue to do so.

The graduate life at UCR is never boring. Well, maybe sometimes a bit in terms of temporarily being stuck with the paper writing, but that usually fades away quickly. For most of the part, I am glad to be able to embrace the life back to campus. In the end, there are sentimental emotions because of the best memories with the people here. I had pleasant experiences attending Professor Ertem Tuncel's course and enjoy talking with other faculties such as Profs. Jie Chen and Jianlin Liu. They've been so approachable and willing to listen and offer advice. The lectures by Ertem are not only a sharing of knowledge but also a convey of outlooks towards life, community and awareness of the nature. This is one of the best parts about the university. You learn to care for something more than one's own world. Because of this, I would also like to extend my gratefulness to Prof. Brandon Lattu. We worked together in the spare time to showcase in an artistic way how the energy saving LEDs can change the life, which was an amazing experience.

I'm also fortunate enough to make so many friends. Ning Liu has always been

encouraging and sharing his experiences to handle the stress and concerns in life. During the days of my internship, Kaiyun Cui gave me a hand to take care of my CPT renewal and OPT application whenever I needed his help as a friend to count on. During past days, I'm also pleased to know Feras Abou-Galala, Gang Chen, Haipeng Ding, Leijie Wang, Li Wang, Michael Leonardi, Yiyang Li and Zongyu Dong who worked with me in the same lab.

It was during the internship at Broadcom Corp. that I learnt a lot from my supervisor Dr. Jianping Peng in his unparalleled passion of work. He discovered my resume and mentored me from the start to the finish. Knowing my work was delivered to the hands of hundreds of millions of Iphone users brings me such a rewarding sense of achievements.

Last but most important of all are my families' faith, support and love. In the past five years, my parents Hongmei Feng and Weiwang He sacrificed in a unthinkable way to bear with the days without their son by the side. When I was away from home, they held me from anything that might be concerning and distracting. In some of the occasions when they needed me most, I was not able to make it unfortunately. This is what I feel afflicted and so regretted with. I know I'm living their best wishes and expectations. I'm doing every means not to let them down. My wife, Xiaoting Cui is the best gift I can have in my life. All through these years, we went through ups and downs together. Her love is unselfish, pure and persistent. Her kind personality is what mirrors me to be a better man. For their unconditional love and care, I dedicate this thesis to my families.

To my families.

ABSTRACT OF THE DISSERTATION

Performance Limits of Outdoor Wireless Optical Communication Links through Scattering and Turbulent Channels

by

Qunfeng He

Doctor of Philosophy, Graduate Program in Electrical Engineering
University of California, Riverside, September 2012
Professor Zhengyuan Xu , Chairperson

Scattering and turbulence are two major obstacles posed by an optical channel to an outdoor wireless optical communication (WoC) system. This thesis is devoted to studying their effects on the performance limits of two typical communication systems in terms of the error probability and outage probability. One is the so-called non-line-of-sight (NLOS) scattering communication system such as a ultraviolet (UV) system, and the other has a line-of-sight (LOS) transmission path, such as an infrared (IR) point-to-point communication system that falls into the category of free space optical (FSO) links.

With regard to an NLOS communication link, the author characterizes the scattering phenomena in terms of the channel path loss and impulse response models. By integrating an empirical path loss model, an NLOS UV communication link is comprehensively investigated for the first time to reveal its potential, and fundamental tradeoffs of communication range versus data rate are reported. In addition, in view of realistic transceiver implementation options, the author effectively takes into account typical device probabilistic models and reveals system performance. Corresponding findings present more realistic insights into NLOS UV system design, weighing over device

choices and tweaking the key parameters.

For an LOS FSO link over the range above 1km, the turbulence effect tends to overshadow the system performance. Traditionally, techniques such as error-control coding (ECC) and spatial diversity have been introduced to enhance a FSO link. By contrast, the author has proposed a novel opportunistic cooperative relay structure to improve the FSO link performance. It is shown the cooperative scheme indeed ensures more robust transmission through an information theoretic analysis.

Along with the analytical study, the author adopt both numerical methods and Monte-Carlo simulation to illustrate the performance limits and advantages of the proposed methods and scheme. The results are expected to provide valuable reference to link budget and system design.

Contents

List of Figures

List of Tables

Chapter 1

Introduction

1.1 Background of Wireless Optical Communications

The earliest form of wireless optical communications (WoC) can be traced back when human beings lit up fires and smoke to alarm the invasion of intruders. Nevertheless, it was not until late 19th century when Bell filed a patent on the concept of "photophone" and prototyped the apparatus able to convey the voice over 200 meters. The community remained inactive since then until the time wheel rolled into 20th century, when the theory, components and system integration technology became more mature. On the other hand, people have been seeking more efficient and effective ways of communication because the traditional radio frequency (RF) based wireless communication and other applications rendered the spectrum unprecedentedly crowded. The first achievement in the optical communications happened to based on the fiber with lower insertion loss medium which had been long envisioned by the Nobel Laureate Sir. Charles Kao. Optical sources such as light emission diode (LED) and solid state laser (SSL) entered into mass production with smaller size and higher emitted optical power. In a word, the developments in the fields of optical channel, sources, detectors and the-

ory of communications have propelled academia and industry to review the feasibility of wireless optical communications which may provide free-licensed, easy-to-deploy, high throughput wireless data access.

A WoC link is comprised of an optical transceiver at the transmitter side and one at the receiver side, each of which needs additional optical front end including a lens, filter and optical source. Several link configurations are possible in terms of the link geometry. In general, when the source is pointed directly towards the receiver aperture, a line-of-sight (LOS) path is created, which is also referred as free-space optical communications (FSOC). Other scenarios for WoC can be directed, non-directed and non-line-of-sight (NLOS) implemented by the adoption of an LED source with large beam angle and aided by some unique channel conditions. In what follows, we first introduce the key system elements of a WoC link such as the source, photodetector and channel. Then we elaborate the motivations of the research, relevant work and contributions of the major thrusts of this thesis.

1.1.1 Optical Source Characteristics

As a category of wireless systems, a WoC link shares a similar architecture as a RF system consisted of a transmitter, channel and receiver. Discussion on the physical layer performance relies on a comprehensive understanding in the characteristics of these components to abstract and formulate theoretic models. An optical transmitter stimulates the source to convert electronically modulated signal into optical field, which is illuminated into the atmospheric channel through the optical lens. By analogy, the optical front end with a lens acts in a similar way as the antenna to a RF system. As for the optical source, a laser diode (LD) or LED may be the candidate. Distinct as the underlying physics that determines the beam and the purity out of the source,

both provide certain amount of optical power as large as hundreds of milliwatts even up to watts, while being small in size and convenient to be driven by a simple electrical circuit. On the other hand, based on the input-output characterization, LED typically maintains good linearity and has limits on the peak power while the LD is more suitable for transmitting the optical power in a fast gated fashion. Hence it is usually adopted for high speed pulse based modulation [24]. For some LDs, the highest gating speed can reach $10Ghz$ and with the external modulator such as the MachCZehnder modulator (MZM) modulator, the speed can be even higher. Overall in the context of optical communications, the optical source can provide reasonably large overall system bandwidth, and the generated pulse can have arbitrarily fast transition between ON (high) and OFF (low) states (levels).

1.1.2 Photodetector Considerations

At the receiver side, a photodetector is a crucial device to generate electrical signals in response to every portion of the optical power impinged onto the photo-detecting material. To characterize, sensitivity, response speed, quantum efficiency and dark current are all the critical factors that determine the ultimate performance of an optical communication receiver. Typical photodetectors can be categorized into a p-n photodiode, photoconductor, photomultiplier tube (PMT), and avalanche photodiode (APD) [5].

The first two devices share the same concept in that photon absorption results in a photocurrent proportional to the incoming optical power. A p-i-n photodiode is manufactured by sandwiching an intrinsic layer of semiconductor lightly doped with donor atoms to a certain density, which helps to boost the quantum efficiency (QE) of photo-electron conversion. Along with the QE are two other important metrics of the

detector performance, namely, transit time and capacitance. The transit-time is directly associated with the time of carriers traversing the depletion region (contained in the intrinsic layer) and the capacitance is determined by the permittivity of the material and size of the depletion region. The evaluation of photodiode has to weigh over the tradeoff between transit time, capacitance and QE since they are inter-dependent.

Of special interest to our research are PMT and APD for their capability to detect a very weak optical signal. A PMT is a vacuum tube which has a photocathode responding to the arrival of primary photoelectrons and an electric field is further applied to accelerate the generated electrons towards a series of dynodes. Each dynode may be stimulated to emit several times more secondary electrons so on and so forth, and the whole multiplication process thus provides a huge gain as high as 10^6. Meanwhile, PMT has a very quiet output with an extremely low dark counts. For its cons, one needs to be aware of the fact that such a high gain is random in nature since each amplification stage has a variation fluctuating from time to time. For another, multiple cascaded stages in a PMT cause a much longer response time which implies a narrower bandwidth. A typical PMT has a bandwidth of several hundreds of MHz. This can impose a limit on some high speed communication applications, let alone the size constraint due to the vacuum tube and high bias voltage to maintain the electric field. In short, the PMT characteristics of high sensitity and low noise make it pretty suitable for implementing a photon counting receiver which counts the incoming number of photons for signal and noise before decision, during the process of which Poisson distribution is a natural reflection. This is a fundamental premise for the theoretical study within the framework of Poisson communication theory [66]. We shall see in the following discussion that the approach to derive Poisson statistics based results can be discrete in nature, largely distinct from the continuous Gaussian assumption.

APD is oriented from the ordinary photodiode with the capability of generating many electron-hole pairs in response to the absorption of even a single photon. The process resembles that of PMT but the physics is to manipulate a PN junction with a unique doping profile comprised of four sections. When a reverse bias is added, Zener breakdown mechanism is employed to regulate the diode and the avalanche breakdown is triggered to generate more electrons through an ionization effect. A typical APD has gain from a few of tens to several hundreds. Similar to PMT, the inherent amplification process is statistically random and output photocurrent thus experiences variations, the effect of which is defined as so-called APD excess noise. As a silicon based photodiode, APD reacts much faster than PMT does but produces much more noise. The fact leads to the treatment of the noise as the thermal white Gaussian noise (AWGN).

1.1.3 Atmospheric Optical Channel

Understanding of light propagation through the atmospheric channel is undoubtedly the most significant foundation for the study of the WoC system performance. However, it is less possible to investigate the optical channel without a big picture of the light spectrum and the well established concept of wave particle duality from the theory of Quantum mechanics. In general it is close to saying the longer the wavelength is, the more a light beam can be studied in the perspective of the wave property while the shorter the wavelength is, the more interactions of photons with the medium are becoming much interesting.

When a light wave propagates, the atmosphere generates random irregularities in the refractive index of medium. Turbulence effect applies to the light beam and causes the distorted wavefront, beam spreading, beam wander and scintillation of the received intensity. By Kolmogorov theory [26], the turbulence causes fluctuations in refractive

index, which can be described using a correlation function between the indexes at two separate locations $\bar{r}_1, \bar{r}_2$ and time instants t_1, t_2

$$\Gamma_n(\bar{r}_1, t_1; \bar{r}_2, t_2) = E\Big[n(\bar{r}_1, t_1) \cdot (\bar{r}_2, t_2)\Big], \tag{1.1}$$

where $n(\cdot, \cdot)$ is the variation function of the refractive index. When $t_1 = t_2$, the above equation is named as spatial coherence of the refractive index $\Gamma_n(\bar{r_1}, \bar{r_2},)$. Its Fourier transform $\Phi_n(\bar{k})$ is defined as the wavenumber spectrum proposed by Kolmogorov

$$\Phi_n(\bar{k}) = 0.033 C_n^2 k^{-11/3}. \tag{1.2}$$

C_n^2 is the wavenumber spectrum structure parameter and depends on altitude and strength of turbulence, with $10^{-13} m^{-2/3}$ for strong turbulence while $10^{-17} m^{-2/3}$ for weak turbulence.

The channel effect on the optical field can also be quantified directly through the analysis of spatial and temporal coherence. By employing the Rytov method, optical field $u(\bar{r})$ is expressed in its amplitude $A(\bar{r})$ and phase $\phi(r)$ such that

$$u(\bar{r}) = A(\bar{r}) \cdot e^{j\phi(r)} = u_0(\bar{r}) \cdot e^{\Phi_1}, \tag{1.3}$$

where $u_0(\bar{r})$ is extracted as the optical field undistorted by the turbulence. The second part Φ_1 hence reflects the turbulence effect and can be written as

$$\Phi_1 = X + jS. \tag{1.4}$$

X is the log-normal variation and S is the phase change. For a wireless optical link with a distance from a few hundred meters to tens of kilometers, the optical field is no longer constant when it reaches the lens at the destination. An optical receiver must be able to overcome the fading effect caused by such a random fluctuation in order to make a reliable decision. One of the objectives of this thesis is to explore ways of offering diversity against turbulence induced fading.

Although the turbulence has a detrimental effect built up over relatively longer distance for longer wavelength (on the order of 1000nm), scattering and absorption are the challenges to short range communications using shorter wavelength. Root causes of the scattering are the aerosols and molecules in the atmosphere formed from haze, fog, rain and cloud. Mie theory was adopted to describe the complex scattered optical field for any outgoing direction from any incidence direction, and the change of the direction is largely due to the physics when a photon is absorbed and released. In the event of multiple scattering, dispersion in angle of arrival for a beam can be on the order of tens of degree. Besides, a rich number of paths of transmission cause the light pulse expanded in time, the effect of which is called pulse dispersion.

To conclude, depending on the scenario, channel characteristics can be largely distinct and the channel acts on the optical field either in the form of the turbulent effect or scattering effect. The analysis and development work need to distinguish and coin these features into the problem formulation before any conclusions can be drawn.

1.2 Some Important Concepts

We will review several important concepts and topics relevant to the study of a WoC system performance in this section. The so-called intensity modulation and direct detection (IM/DD) is the major signalling and detection scheme for optical communications especially the WoC. The model of Poisson communications is an abstraction on the scenario, which characterizes the statistics of the photodetector output. Moreover, the speciality of a wireless optical channel may cause the fading in signal power. Hence we present fundamentals on the methodology of analysis in the presence of randomness resulted from fading.

1.2.1 Intensity Modulation and Direct Detection

By IM/DD, the transmitter modulates the intensity of optical field. It shall be noted that IM is a practical modulation scheme, especially true for an LED based optical source. Unlike the light generated by a coherent source such as Laser, the LED does not guarantee a pure and uniform property in the phase, and polarization of the optical field. For UV communication, traditionally the intensity based modulation is the only feasible choice. To modulate the intensity, the constellation can be in the binary level or multiple levels. A binary modulation employs a non-return-to-zero (NRZ) pulse during a time slot to represent the bit one and holds off the transmission during the time of bit zero. A multi-level modulation can be implemented either through manipulating multiple intensities or orthogonal positions of a pulse.

A direct detection receiver is also named as non-coherent detection which is in contrast to coherent (heterodyne) detection. The latter usually calls for a local optical source generating a spatially aligned field with a wavelength λ_L only within a small fraction of that of the received optical field. Since the mixing process generate a RF signal with a non-zero carrier frequency, a heterodyne method is robust against background radiation. When a high performance photodetector and amplifier are commercially available, the background noise can be substantially reduced. In addition, considering the fact that non-coherent detection does not require local light source and largely excels in its simplicity, it is a more natural choice for system designers.

According to the physics of a photodetector, the device output is a current stimulated by the incoming photons. To process in the electrical domain, the detector is first loaded by an output impedance R_L which produces the corresponding voltage signal $v(t)$. The signal may be further filtered and integrated over a modulation symbol

period before the decision unit decodes using maximum likelihood (ML) or maximum a-posteri (MAP) methods. More details will be provided in Section 1.2.3.

For the photodetector in a DD receiver, it behaves as a "square law" detector responding to the optical field envelope. This is one of the fundamental differences from the antenna in radio frequency (RF) realm. Note the incoming optical field includes both signal field and background noise, which can be expressed as

$$a(t) = s(t) + b(t), \tag{1.5}$$

where $a(t)$ is the complex envelope of the received field $f(t, \mathbf{r}) = |a(t)|e^{j\omega t}$. Because of the "square law" and assuming single mode optical field, the photondetector has a detection output with the count rate process as

$$n(t) = \eta A|a(t)|^2. \tag{1.6}$$

η is the quantum efficiency of the photodetector and A is the area of photosensing material; $n(t)$ is the random photon count process with a time average as,

$$\begin{aligned}\bar{n} =& E[\eta A|a(t)|^2] = \eta A\overline{[s(t) + b(t)][s^*(t) + b^*(t)]} \\ =& \eta A(I_s + I_b), \\ =& \eta(\lambda_s + \lambda_b).\end{aligned} \tag{1.7}$$

In the above, λ_s represents the signal photon count rate and λ_b is the rate of background radiation. As a result, background noise is additive to the received signal in the IM/DD model.

1.2.2 Poisson Counting Receiver

The second important concept in our study is the Poisson counting receiver (or photon counting receiver). Through last section, it is clear the output of a photodetector

is equivalent to a photocurrent directly proportional to the photon arrival rate since the level of photon current is the joint contribution of the photonelectrons (PEs) released by the photon-sensing material after absorbing the arriving photons. A semiclassic approach adopts the probabilistic principle to depict the interactions of photons on the detector. It is determined the process is random in nature and the emissions of k PEs follow Poisson distribution

$$P(k) = \frac{m_T^k e^{-m_T}}{k!}. \tag{1.8}$$

By counting the electrical pulses, each of which can be attributed to the release of one PE, the receiver collects decision variables during a specific period T. In the eqn. (1.8), $m_T = \bar{n}T$ is the mean count of PEs due to the photon arrivals during T.

As a matter of fact, when the received optical field has a random variation in the intensity, the count m_T itself is a random process as well. In a more general context, the model of receiver count $K_t, t \geq t_0$ is described as a doubly Poisson counting process and the intensity function $n(t), t \geq t_0$ is a stochastic function [62]. To state otherwise, $K_t, t \geq t_0$ is an integer valued process with independent increments such that during time (s,u]

$$Pr\{K_u - K_s = k | n(t), s < t \leq u\} = \frac{\left(\int_s^u n(t)dt\right)^k \exp\left(-\int_s^u n(t)dt\right)}{k!} \tag{1.9}$$

For a wireless optical system, eqn. (1.6) may be rewritten as below by capturing the channel random scaling effect $h(t)$ and the gain G control of the photodetector

$$n(t) = \eta G h(t) s(t) + b(t). \tag{1.10}$$

If $h(t)$ is a random process, then $n(t)$ is the function of a random variable and the distribution of the instantaneous counts k has to be expressed as a weighted function,

$$P(k) = \int_0^\infty \frac{m_T^k e^{-m_T}}{k!} p_h(h) dh, \tag{1.11}$$

where $p_h(h)$ is the distribution density of the atmospheric channel.

Lastly, not only the channel property might change the count statistics of a DD receiver, but also the photodetector's gain level G might alter the game in that Poisson distribution might no longer be applicable. To offer more insights on how the component plays a role in the performance, we shall revisit this topic in Chapter 3 on how to construct a statistical model of the receiver output for performance analysis.

1.2.3 Figure of Merits: BER and Outage

To evaluate the performance limits of a WoC link through the scattering/turbulent channels, one can choose to derive the error probability as the system performance measure on how good the communication quality is, or the outage rate on how robust a certain data rate can be maintained. The principle and purpose of error analysis of a WoC system resemble any digital communication system in answering the question of whether a transmitted modulation symbol becomes erroneous at the receiver. It is true most of contemporary modulation schemes such as phase/amplitude/frequency shift keying (PSK/ASK/FSK) have been thoroughly studied in the RF community. When it comes to the context of wireless optical communications, some fundamental system aspects are so different that results of RF modulations can hardly be extended and applied. Admittedly, the definition of symbol error probability (SER) [35] is

$$P_{e,sym} = Pr\{\hat{s}_m \neq s_m | s_m \ is \ sent\} \tag{1.12}$$

The error probability for typical modulations over an additive white Gaussian channel (AWGN) can be developed in closed forms by taking advantage of the Q-function. And the optimal receiver structure can be obtained through maximization of signal-to-noise ratio (SNR). Matched filter is an example given the definition of signal representation.

In contrast, we will develop our BER/SER model built upon the unique assumptions for WoC systems and the baseband pulse based intensity modulations in this thesis.

Besides error probability, another measure is the outage probability which is especially a reasonable measure when a wireless communication link undergoes a random change of the channel caused by the fading effect. In the presence of deep fades, the error probability or the instantaneous capacity is compromised enormously because SNR has a substantial loss. If we specify a minimum requirement on SNR Γ_{th}, outage probability is defined as the probability that SNR Γ falls below Γ_{th}. Note that, given the signal representation, SNR can be expressed as a function of the channel condition h as $\Gamma(h)$. Hence we have [61]

$$P_{out} = Pr\{\Gamma(h) < \Gamma_{th}\} = \int_0^{\Gamma_{th}} p_\Gamma(\Gamma) d\Gamma. \tag{1.13}$$

When SNR $\Gamma(h)$ can be inverted such that $h_{th} = \Gamma_{th}^{-1}$, the above equation can be further expressed as

$$P_{out} = \int_0^{h_{th}} p_h(h) dh. \tag{1.14}$$

1.3 Motivation and Prior Work

We aim to investigate the performance limits of an outdoor wireless optical communication link through scattering and turbulence. Two ranges of wavelength are of intense interests. One belongs to the ultraviolet (UV-C band: $200-280nm$) while the other is in the infrared band (IR: $1260-1675nm$). As aforementioned, optical channel assumes much different characteristics in these two wavelengths since the scattering signifies the light propagation loss in the UV band and the turbulence poses an enormous fading effect on the IR based free space optical (FSO) link. Such a difference is exploited to apply UV and IR technologies to two specific scenarios considering the nature of light

propagation. IR is appropriate for a medium to long range FSO communications because the the commercial-off-the-shelf (COTS) devices are available thanks to the leverage from the great leap in the field of fiber optical communications. Hence, our main focus is on how to design an effective and robust communication link against turbulence induced fading. When it comes to UV range, the technology starts to become an eye-catcher not until recent years when more findings on the channel and its advantages were revealed [74]. In view that the research on UV communications is still in its infancy, we are more intrigued to answer some of the fundamental questions regarding the potential of the UV link.

1.3.1 NLOS UV Communications over Scattering Channel

Communications in the UV-C wavelength range benefit from the unique properties of a UV channel. The scattering effect becomes stronger when the wavelength is close to the size of atmosphere constituents on the order of $200nm$, which renders possible the transmission of light signal through a non-line-of-sight (NLOS) path and relaxes the strict requirement on pointing, acquisition and tracking (PAT). What's more, in the UV-C band, because of the protection of the ozone layer, only 1 percent of solar radiation is expected near the ground. Hence an optical receiver with a large field-of-view (FoV) is feasible to collect as much optical power as possible without being jeopardized by the strong background noise. The flexibility of link configuration and its low noise advantage enormously inspire the community to study the UV link. Early and recent works in the literature [15], [53], [58], [59], [60] can be classified into three aspects: devices, channel and communication. The advances in the first two areas ultimately facilitate the new results in the analysis of communication performance.

In the field of device technology, several early experimental systems were re-

ported and dated back to 1960s when xenon flashtube was used as a UV source with very high power. Soon after that, an NLOS UV system based on the UV lamp was implemented in 1976. Light sources of UV lamp, flashtube and laser are mostly bulky, power consuming and speed limited. A semiconductor UV source has drawn much attention as a consequence of the funding projects of Defense Advanced Research Projects Agency (DARPA). Commercial UV LED or LED array debuted not until ten years ago [3], [57] and an optical power up to $50mW$ can be emitted in the UV-C band. With regard to the photodetectors, there are commercial PMTs from Perkin-Elmer and Hamamatsu Photonics. Intense research efforts persist in the development of APDs in the deep UV band under the support of DARPA's deep UV APD program (DUVAP) [8].

A UV channel especially in the NLOS scenario has been adequately studied in recent years through experiment validation, theoretical derivation and Monte-Carlo simulation. Due to the scattering effect, NLOS propagation is possible but a substantial path loss can be caused as the elevation angles of a transmitter (tx) and receiver (rx) and their separation distance vary. There have been numerous attempts to characterize the path loss mainly based on single scattering modeling or approximations under large apex angles [46, 59, 71, 73]. Recently some Monte Carlo techniques are suggested to simulate the multiple scattering effects on path loss [20]. Also an empirical path loss model validated by field experiments is proposed [16]. The model is presented by tabulating the path loss exponents and attenuation factors for different link geometries.

By combining the elements of realistic device model and knowledge on the channel such as path loss, we are motivated to determine the performance limits of an NLOS UV communication link in terms of achievable range and rate. Traditional way of the investigation in this field relies on experimental characterization and field demonstrations. Targeting on a low power short range NLOS UV link, there have been

very few articles devoted to developing an abstract model which captures the channel, photodetector and noise sources comprehensively. Results and predictions reported in this thesis have helped to develop a multiuser system such as an ad-hoc like sensor network by extending the single user case.

1.3.2 LOS FSO over Turbulent Channel

The IR technology has been commercially applied to construct long range LOS FSO point to point link in both civilian and military purposes. The majority of IR based FSO systems adopts transmission windows in either $780-850nm$ or $1520-1600nm$ due to device considerations. In the range of $850nm$, most COTS components are available for transmitters and receivers using the silicon based APD detector technology while wavelengths around $1520nm$ are more suited for FSO transmission with a less strict requirement on eye safety. It is reported that roughly 50 times more power can be illuminated with $1520nm$ than what can be allowed in $780nm$. Aided by the erbium-doped fiber amplifier (EDFA) technology, a transmitter can even support higher power and data rates.

FSO links can be used in many civilian and military applications. In some scenarios, it is mounted on top of the buildings for a metropolitan network where the challenge lies in the pointing and acquisition due to building sway. In other applications, the FSO links are integrated into UAV/satllite platforms for communication over $10km$ in the atmospheric channel. Fog, rain and cloud cause the light signal severely attenuated while the scintillation effect distorts the wavefront randomly [6], [41]. Solutions based on the communication techniques have been proposed to overcome the challenges, and most of them yield well established theoretical abstractions. As a physical layer approach, error correction codes have been adopted to enhance the performance using

block and convolutional codes. Iterative decoding for LDPC codes has been employed and discussed [7], [9], [21], [25]. In view of the distinct channel properties in optical wavelength and RF, a hybrid solution combining adaptive scheduling of transmission over an optical-RF parallel link is also studied in [44], [48].

Instead, we are interested to explore other potential technical solutions to overcome the channel fading effect on a FSO communication link.

1.4 Contributions and Outline of the Thesis

Our study of NLOS UV communications is built upon the experimental investigation and modeling of the scattering channel. We also quantify the pulse delay spread due to the scattering, and analyze how performance is degraded under the inter-symbol-interference and noises from solar radiation and devices. Theoretically, the NLOS UV communication link is modeled assuming a Poisson counting receiver and the Poisson statistics for the incoming light signal. The contributions of our work related to UV communications are reported in Chapters 2 and 3.

Chapter 2 introduces the UV communication system structure. The prior work in scattering channel has provided predictions on the path loss and temporal response. Based on an optimal maximum likelihood (ML) receiver model, the author has integrated the channel model to theoretically predict the error performance for an NLOS UV link, which extends the experimental demonstration reported in Chen/Shaw's work. Fundamental tradeoffs such as range versus rate have been revealed through our study and thus facilitates the link budget. Furthermore, we consider a more realistic case when data rate is increased and the pulse dispersion causes inter-symbol-interference. Since the photon counting model in our analysis prevents the direct application of the

methodology of ISI study that has been used in RF domain, we propose an approach to project the contribution of ISI into each decision period and the resulted performance loss quantitatively. Lastly, since the LED array serving as the light source can be quite restricted in power, the concept of a multihop NLOS UV link is proposed for the first time to extend the range of communications while previously it was examined for the LOS case [4]. We further identified the spatial interference issue associated with the configuration and provide a time division based multiuser access control (MAC) protocol. It is shown the proposed method can effectively minimize the interference.

In *Chapter 3*, both PMT and APD models are considered in the performance analysis, which is a step forward beyond the content introduced in Chapter 2. Here, the photodetector is a part of the receiver electronic circuit with a trans-impedance amplifier. Thermal noise is introduced and added to the dark current, the random gain variation and background radiation, which largely downgrade the system performance. Our contribution is in that we derived a statistical model to combine above Gaussian noise sources with the Poisson statistics. Such a mixed Gaussian and Poisson scenario is unique to the NLOS UV communication receivers with highly sensitive photodetectors and was formally treated in our discussion. We point out the excessive noise of APD is relevant to the gain settings, hence there is an optimal gain that can be chosen to reach the minimum error probability.

A major challenge to the LOS FSO IR communication is the turbulence induced fading. *Chapter 4* explores a user cooperation technique to improve the link performance. In literature, it was not until recently that FSO scholars started to investigate the benefits of relay and relay based user cooperation against the fading effect. For example, noticing the fact that turbulence is distance dependent, Safari-Uysal first formulated a mathematical model on FSO serial and parallel relayed links in [54], where

the number of relays can be arbitrary. In a three-way system scenario, Karimi [39] derived the BER performance of a cooperative FSO link enhanced by convolutional code and Abou-Rjeily [1], [2] obtained semi-analytical results of BER performance assuming ideal photon counting model. Our research complements the results derived using a photon counting model by assuming a Gaussian noise dominant infrared link. The user cooperation gets involved in an opportunistic way rather than deterministically, which enhances the link robustness when the channel condition from the source to the relay deteriorates. In our setup, the relay can be in either a decode and forward (DF) mode or amplify and forward (AF) mode.

Chapter 5 highlights the contents and major results of the dissertation. Our work builds a solid foundation in the NLOS UV communication and FSO link level technologies for other topics involving multiple users, namely, the k-connectivity issue and medium access control. The problem formulations and numerical methodology may be well applied or extended to the relevant studies of WoC systems.

Chapter 2

Fundamental Tradeoffs in a Scattered NLOS UV Link

The performance of NLOS UV communication through a scattering channel has not been systematically investigated in literature before our work. The chapter considers the unique features of UV communications such as low noise, high sensitivity and scattering effect and obtains the knowledge on the potential of a short range NLOS UV channel for communications. The study is developed on the assumption of an ideal photon counting receiver. The methodology is to combine into the symbol error equation the path loss model and pulse delay spread which are two most significant characteristics of a scattering channel. Due to the scattering, the optical power has substantial loss before it reaches the receiver aperture; on the other hand, rich scattering creates multiple path of transmission such that the light pulse is expanded. The analysis of link performance has to take into account these two specific aspects.

In what follows, Section 2.1 presents several preliminaries which are necessary bricks to construct our framework of modeling. Section 2.2 touches the fundamental

question on what is the achievable rate versus range constrained by the given error performance. To improve the limited range of communication due to huge path loss of the NLOS UV channel, we propose the concept of a multihop NLOS WoC link to the UV communications in Section 2.3. Section 2.4 reports the numerical results and findings.

2.1 Preliminaries of UV Communications

2.1.1 An NLOS UV System Configuration

Similarity as an NLOS UV link shares with any WoC system or wireless communication link, the system configuration has its special attributes of flexible geometric link configurations which are illustrated in Fig. 2.1. Here V is defined as the transmitter

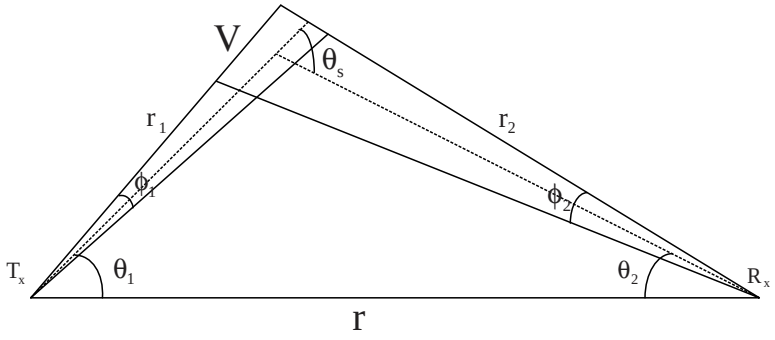

Figure 2.1: A NLOS UV communication link.

(Tx) and receiver (Rx) common volume; theoretical study in literature suggests the path loss is related to the volume size. r is the Tx and Rx baseline separation. r_1 and r_2 are the distances of the common volume to the Tx and Rx, respectively. Define θ_1 and θ_2 as the Tx and Rx apex angles between the corresponding axis and the horizontal axis, and ϕ_1 and ϕ_2 as the Tx full beam angle and Rx field of view (FOV).

A NLOS UV communication system adopts the intensity modulation and di-

rect detection (IM/DD), for which the intensity of light is manipulated to represent modulation symbols. Although the background radiation remains a substantially weak level, solar blind filters of 255nm and 271nm can be placed in front of the UV enhanced PMTs such as the Perkin Elmer MP1922 and Hamamatsu R7154 to further reduce unnecessary response to the out-of-band light field. The NLOS UV test bed implemented at the wireless information technology lab (WITLab), University of California, Riverside selects commercial UV LEDs at the wavelength of either 280nm or 250nm as the light source. In the wavelengths of interests, the spectrum on the chosen wavelengths is measured to have a minimum solar irradiance near the ground [72].

2.1.2 Characteristics of NLOS UV Scattering Channel

UV channel experiences extinction, absorption and especially the scattering effects. For the purpose of link budget, it is highly necessary to characterize the channel path loss model, which can be treated as the channel DC gain $H(0) = \int_{-\infty}^{\infty} h(t)dt$, then the received average optical power is expressed by $P_r = H(0)P_t$. Some experimental and analytical results about the NLOS UV channel path loss model have been documented in [16], [72], [73]. It is proposed in [16] an empirical model reflecting the path loss $L = \frac{1}{H(0)}$ in relation to above parameters for r within the range of 1km, which is described as

$$L = \xi r^{\alpha}. \tag{2.1}$$

In eqn. (2.1), ξ is the path loss facor and α is the path loss exponent, which can be determined through the lookup tables obtained from the outdoor experimental measurements. The value of α ranges from 0.45 to 2.4 depending on apex angles and baseline separation. It is found for large apex angles, α is prone to assume smaller values. Tables. 2.1 and 2.2 tabulate the model in terms of ξ and α corresponding to different Tx and

Rx apex angles.

Table 2.1: Path loss factor ξ of NLOS UV channel.

θ_1@Tx \ θ_2@Rx	20°	30°	40°	50°	60°	70°
20°	3.43e5	1.97e6	1.13e7	2.28e7	7.59e7	2.98e8
30°	1.41e6	8.54e6	7.34e7	1.24e8	4.01e8	1.10e9
40°	2.97e6	1.74e7	1.69e8	2.53e8	6.55e8	1.17e9
50°	2.92e6	1.06e7	1.09e8	1.83e8	4.85e8	8.86e8
60°	5.42e5	3.30e6	3.15e7	5.38e7	1.71e8	5.21e8
70°	4.94e6	2.60e7	1.83e8	3.07e8	5.82e8	7.35e8
80°	1.90e7	1.30e8	4.76e8	5.66e8	8.56e8	1.18e9

Table 2.2: Path loss exponent α of NLOS UV channel.

θ_1@Tx \ θ_2@Rx	20°	30°	40°	50°	60°	70°
20°	1.9139	1.8359	1.7800	1.6427	1.4641	1.2002
30°	1.8453	1.7219	1.4500	1.3720	1.1340	0.8751
40°	1.8579	1.7091	1.3498	1.2930	1.0559	0.9133
50°	1.7872	1.8310	1.4685	1.3937	1.1543	1.0098
60°	2.4113	2.2737	1.9322	1.8176	1.5264	1.1862
70°	1.9846	1.8581	1.4938	1.3444	1.1581	1.1111
80°	1.8918	1.5259	1.2207	1.1921	1.0474	0.9328

Given the tables, the path loss model can also be plotted in Figs. 2.2 and 2.3, which shows the path loss ranges from $57dB$ to $105dB$ over a range of 100 meters.

The path loss model characterizes the attenuation of scattering channel on the optical power; another critical feature of the channel is the pulse delay spread due to light signals from multiple paths overlapping and rendering a broadened pulse shape. We measured the pulse broadening in [17], which is summarized in Fig. 2.4. The

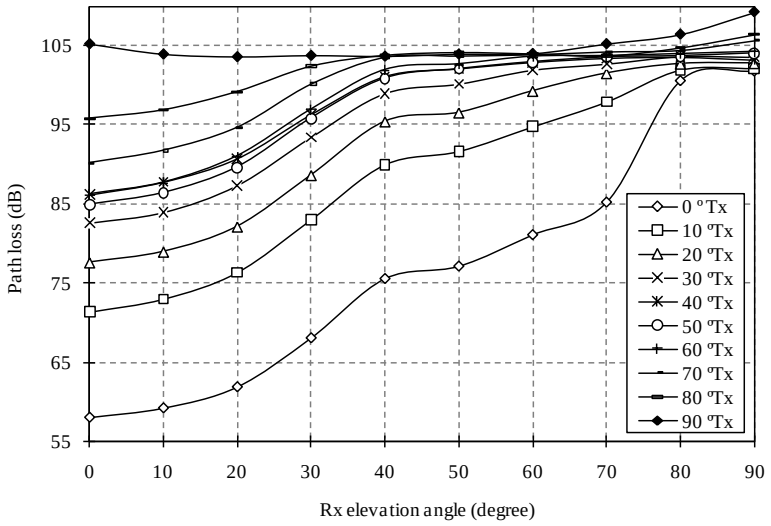

Figure 2.2: Path loss versus Tx elevation angles for different Rx elevation angles [16].

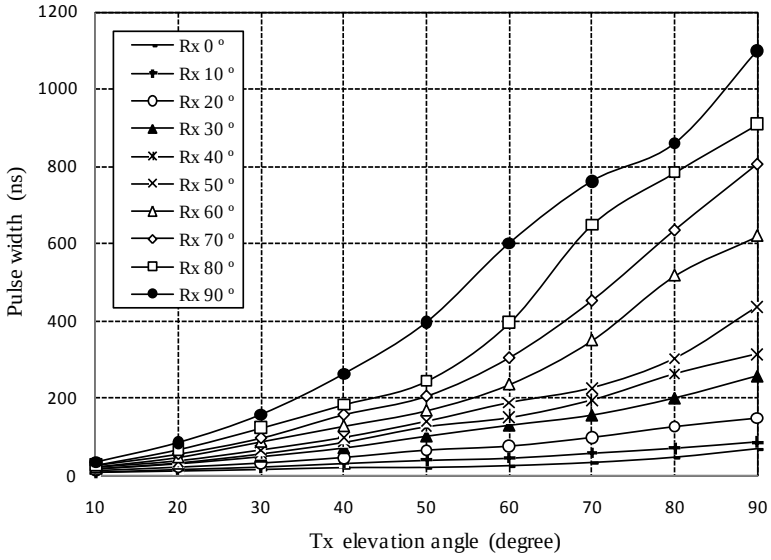

Figure 2.3: Path loss versus Rx elevation angles for different Tx elevation angles [16].

measurement results are under four typical geometries captured by a UV laser based channel sounding platform. Large pointing angles typically cause longer propagation path and thence longer delay spread. Thus the pulse broadening is obviously much severer with larger pointing angles. Figs. 2.5 and 2.6 illustrate the pulse broadening

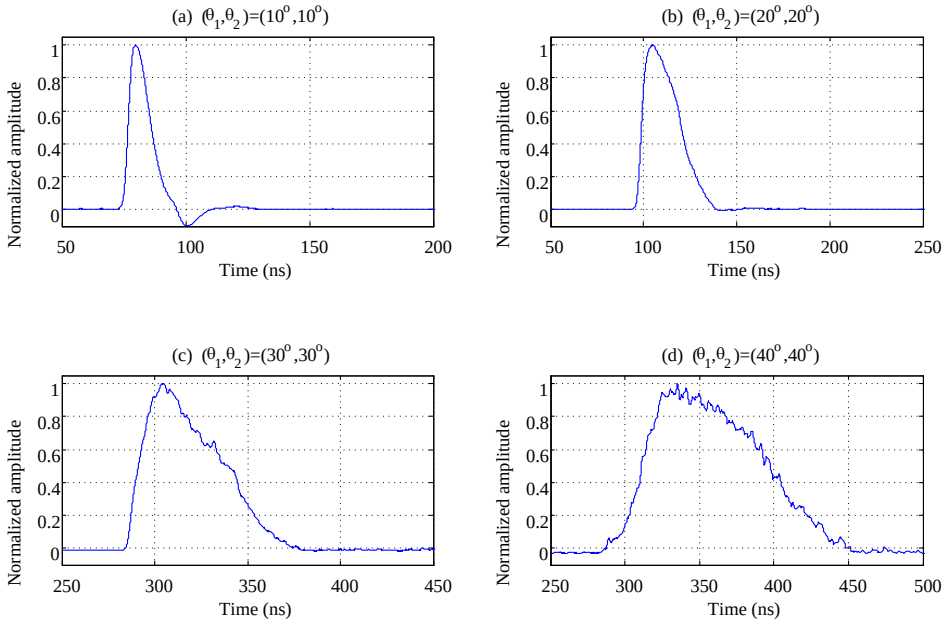

Figure 2.4: Impulse response of UV NLOS channel in four different transmit/receive geometries at 100m.

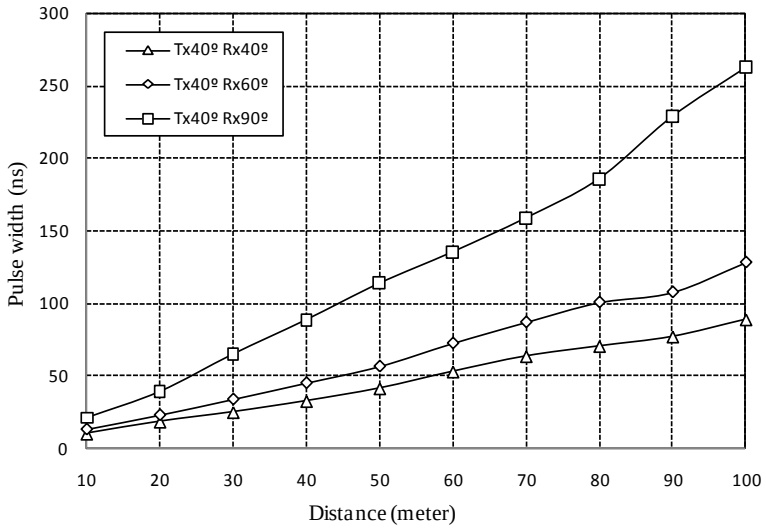

Figure 2.5: Broadened pulse width vs. distance.

versus tx pointing angles and propagation distance respectively. With the increasingly severe ISI effect, a NLOS UV system designer must take cautions on the prediction of system capability and seek measures to improve. In our research, the performance projection and analysis is conducted by considering the ISI effect due to broadened pulse

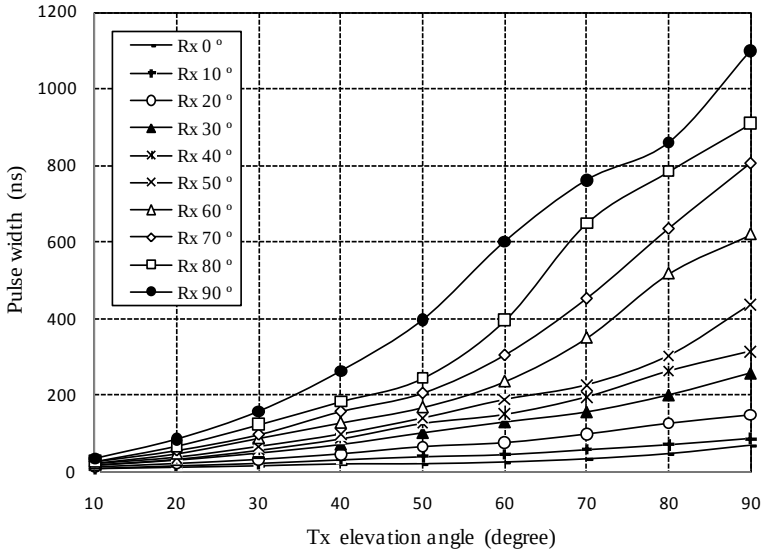

Figure 2.6: roadened pulse width vs. Tx angles.

and the device model. We leave the discussion in the next chapter until we present a comprehensive study on the photodetector dependent receiver design.

2.1.3 OOK and PPM Demodulation by Photon Counting Receiver

Inspired by the low background noise and high rx sensitivity of a NLOS UV link, it is very natural to establish our problem formulation assuming a Poisson photon counting receiver, the output of which is Poisson distributed. Since both OOK and pulse position modulation (PPM) have their modulation symbol represented by the amplitude or position of a baseband pulse (slot), we designate the slot with the signal pulse a signal slot with the time span of T_s. At the photon counting receiver output, the signal photon counts n_s is Poisson distributed with average photon count number of λ_s, which is determined by the instantaneous optical intensity. The average background noise photon count λ_b is mainly contributed by the solar radiation.

The performance of a photon counting receiver to detect the transmitted OOK modulation symbols can be developed by applying the general definition of error prob-

ability as in eqn. (1.12). So we have

$$P_e = \frac{1}{2}\sum_{k=0}^{m_T} \frac{(\lambda_s + \lambda_b)^k e^{-(\lambda_s+\lambda_b)}}{k!} + \frac{1}{2}\sum_{k=m_T}^{\infty} \frac{(\lambda_b)^k e^{-(\lambda_b)}}{k!}. \tag{2.2}$$

The error probability is derived by considering a threshold based detection. The decision unit at the receiver recovers the modulated binary data by comparing the photon counts for each OOK symbol with the pre-defined threshold m_T. If we minimize P_e with respect to m_T, an optimal threshold is given by

$$m_t = \Big\lfloor \frac{\lambda_s}{ln(1+\frac{\lambda_s}{\lambda_b})} \Big\rfloor. \tag{2.3}$$

For simplicity, if the shot noise is assumed to be negligible such that $\lambda_b = 0$ and the optimal detection threshold $m_T = 0$, following result out of eq. (2.2) can be obtained.

$$P_e = \frac{1}{2} e^{-\lambda_s}. \tag{2.4}$$

We also consider the use of optical block encoding [24] achieved by converting every block of b bits into one pulse out of every $M = 2^b$ orthogonal slots. One popular form of such block coding is pulse position modulation (PPM). One of the reasons PPM is favored by communication designer is, first of all, the simple decision rule. The receiver does not need to compute and maintain a threshold, instead compares the photon counts across all slots and chooses the slot with the most counts as a maximum likelihood method in nature. Secondly, PPM is advantageous to recover the symbol clock even when there is a long sequence of zeros. We leave the performance study of PPM modulation in the context of a Poisson counting receiver in the ensuing sections.

To conclude, the understanding of communications through the scattering channel relies on the correct characterization of the path loss and pulse delay spread. The prediction on achievable performance assumes pulse based modulation and photon counting receiver.

2.2 Range versus Rate for Short Range NLOS UV Link

We are motivated to study the topic of range versus rate because the scattering effect dominates the transmission and the path loss for NLOS UV is enormously larger than that of line-of-sight (LOS) link. The two modulation schemes are OOK and PPM and we start with the general case where the background noise is nonzero. Then we derive simple and closed form results for shot noise limited case, which eases the derivation of more intuitional results.

2.2.1 Range-Rate Performance of OOK

Let P_t be the optical power of the LED array and R_b the bit rate. Then $\lambda_s = \eta P_t/(LR_b hc/\lambda)$ where L is the path loss, h is the Plancks constant, λ is the wavelength, c is the speed of light, and η is the combined quantum efficiency of the photodetector and optical filter. Further noting that L is a function of the range and pointing angles as eqn. (2.1), then by substituting it into the expression of λ_s and plugging into above OOK error probability in eqn. (2.2), we can express the range r as a function of bit rate R_b in an implicit way. Since this is a nonlinear equation that relates r and R_b with the rest parameters fixed, including the error probability requirement P_e, noise level λ_b, transmission power P_t, and pointing angles, we can consider tradeoffs between any pair of parameters as a matter of fact.

A numerical approach of computing the tradeoff of range r versus rate R_b can be summarized as below.

- For a given requirement on P_e and measured background noise λ_b, we numerically search for the desired signal photon counts λ_s that achieves the equality of eqn. (2.2) by updating the threshold m_T for each pair of (λ_s, λ_b). The uniqueness in

solution can be justified since the error probability P_e is a monotonous function of λ_s. Classical methods such as binary sectional searching can be employed quite effectively.

- For each determined λ_s, note that it is a simple algebraic function of the range r through the representation of an empirical path loss model. Hence the range r can be computed by inverting the expression of λ_s which contains the bit rate R_b.

- Hence we derive a equation absorbing both the range r and the rate R_b. The variation of R_b within the range of interests leads to corresponding achievable range of communications.

In some special circumstances, namely, at night when the NLOS UV communications link is activated, solar radiation level can be extremely low and a physical intuition is λ_b approaches to zero. Since the photodetector PMT also maintains very quiet in dark current, we could in turn simplify above discussion in a so-called "shot noise limited" scenario. Thus eqn. (2.2) is reduced into $P_e = e^{-\lambda_s}/2$. An expression on the range r as the explicit function of R_b can be determined as

$$r = \sqrt[\alpha]{-\frac{\eta P_t \lambda}{\xi R_b hcln(2P_e)}}. \tag{2.5}$$

In a clearer way of presenting the tradeoff,

$$rR_b^{1/\alpha} = C, \tag{2.6}$$

where $C = \sqrt[\alpha]{-\frac{\eta P_t \lambda}{\xi hcln(2P_e)}}$. Eqn. (2.6) consists in the tradeoff of range versus rate and can be illustrated numerically.

2.2.2 Achievable Performance with PPM

When PPM is adopted as the modulation scheme, the decoder needs to determine which slot of the PPM symbol contains the pulse before demapping it into encoded bits. A decoding error happens when incorrect slot has higher integral value than the correct slot. The symbol error probability of an M-PPM system is given in [24] and according to the relationship between symbol error rate and bit error rate [52], the resulting bit error probability is

$$\begin{aligned} P_e =& \frac{M}{2(M-1)}\left\{1-\int_0^{\infty} p(\nu_1|1)\left[\int_0^{\nu_1} p(\nu_2|0)\nu_2\right]^{M-1} d\nu_1\right\}, \\ =& \frac{M}{2(M-1)}\left\{1-\frac{e^{-\lambda_s+M\lambda_b}}{M}-\sum_{r=0}^{M-1}\frac{(M-1)!}{r!(M-1-r)!(r+1)}\times\right. \\ & \left.\sum_{k=1}^{\infty}\frac{(\lambda_s+\lambda_b)^k e^{-(\lambda_s+\lambda_b)}}{k!}\left[\frac{\lambda_b^k e^{-\lambda_b}}{k!}\right]^r\left[\sum_{j=0}^{k-1}\frac{\lambda_b^j e^{-\lambda_b}}{j!}\right]^{M-1-r}\right\}, \end{aligned} \tag{2.7}$$

where in the first equality of eqn. (2.7), $p(\nu_1|1)$ is the probability density function when correct slot has a pulse and $p(\nu_2|0)$ is the probability density function specifying the rest slots indeed have an integral less than the counts in the correct slot.Note that the relationship between r and R_b for PPM modulation can be readily evaluated numerically. Beware that in M-PPM case, $\lambda_s = (\eta P_t logM)/(LR_b hc/)$ where M is the order of the PPM modulation. When $\lambda_b = 0$, the bit error probability is simplified to $P_e = e^{-\lambda_s}/2$, which is similar to the OOK case except with a different expression for λ_s.

2.3 Extending the Range of NLOS UV using Multihop Technique

Previous discussion has indicated the UV communications leverages the benefits of an NLOS path and covertness of limited range, both ensured by the scattering

channel. Nevertheless, by flipping the coin, there are down-sides such as the huge path loss, which impose unique and harsh requirements on the system design to achieve desired performances in range and data rate. For instance, increasing the power is a common and straight forward method to improve communication performance, but a wireless optical communication (WOC) system must consider the regulations on human eye safety. Also, the convenience of deployment favors light-weight and compact transceivers. The performance of NLOS UV link for communications based on point-to-point transmission has been addressed in section 2.2. In this section, we propose a multihop system configuration to reduce the transmitter power consumption and the number of LEDs while extending the communication range.

Relayed mesh network in radio frquency domain has a rich history and is comprehensively reviewed in [50]. Regarding relayed FSO links, note that there has been some work in recent years [4], [63], [54], but most of them assume line-of-sight (LOS) conditions and focus on outage analysis in a fading environment because of turbulence effects. By contrast, we study the performance of NLOS UV multihop network by incorporating the path loss model specific to NLOS UV channels and neglect the effect of turbulence by restricting the range of each communication link within hundreds of meters. In light of the low noise characteristics of a solar-blind UV system, the performance analysis follows a classical model, i.e., intensity modulation with direct detection (IM/DD).

In what follows, in section 2.3.1, the transmit power with on-off keying (OOK) modulation is obtained for the case of direct transmission as an example illustrating why the NLOS link is power starved. We next obtain the power for individual relay node in a serial multihop configuration using a decode-and-forward scheme aiming to prove the benefit of power saving. We show how the interference in a NLOS multihop system

results from the nature of directional transmission and reception, and the performance degradation is evaluated versus link geometry and the number of hops. Accordingly, a spatial reuse technique of coordinated transmission and cooperative reception is suggested in section 2.3.3.

2.3.1 A Direct Transmission NLOS UV Link

Assuming OOK modulation and shot noise limited case, the number of received signal photon counts during each OOK symbol is $\lambda_s = \eta P_t/(LR_b hc/\lambda)$. Substituting L and λ_s in the above expression using eqs. (2.1) and (2.4), the required direct transmission power for the quantum limited case with end-to-end distance d is found to be

$$P_{DT} = -\xi d^{\alpha} R_b h\nu \ln(2P_e)/\eta. \tag{2.8}$$

This result predicts required power for a given error probability, rate and range. For instance, when $P_e = 10^{-4}$, $d = 500m$ and $R_b = 1Mbps$, P_t is on the order of hundreds of miliwatts. With the state-of-art UV LEDs and commercial off-the-shelf solar blind filter and PMT with a combined photon conversion efficiency η around 6%, the transmitter requires hundreds of LEDs, which is unrealistic in practice. Instead we consider the strategy of adopting a multi-hop link to achieve desired system requirements.

2.3.2 A Multihop NLOS UV Link

Let us examine a multihop topology for a NLOS UV communication link aided by relay nodes in Fig. 2.7. The source transmits an OOK modulated signal to the first relay node through a NLOS channel. Each relay decodes and forwards the received symbols to the next relay and so on. From the source to the destination, there are $N+1$ nodes equally dividing the range of communication into N segments. We specify the

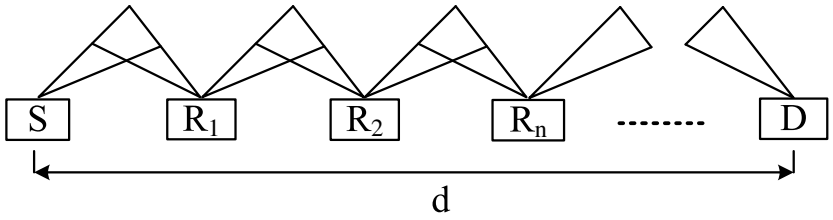

Figure 2.7: A NLOS multihop UV communication link.

same system geometry for both direct transmission and the relaying segments.

To evaluate the transmit power for each node in the serial multihop link, we study the end-to-end error performance $P_{e_{MH}}$ and throughput $R_{b_{MH}}$, equal to P_e and R_b, for direct transmission. With the decode and forward (DF) operation at each relay, it is natural to obtain the end-to-end error performance as

$$P_{e_{MH}} = 1 - \prod_{n=1}^{N}(1 - P_{en}) = 1 - (1 - P_e)^N, \tag{2.9}$$

where P_{en} is the piecewise error probability for the nth hop. The second equality in eqn. (2.9) is established by assuming equal error performance P_e for every hop in the link.

To bridge the power and the error performance, we may simply use eqn. (2.2) as the exact form of photon counting error performance in eqn. (2.9). However, the result will involve summations, preventing any insightful prediction from being drawn. Since the UV system operates in the wavelength of solar blind range and the background noise photons have a very low arrival rate as is reported in [30] to be no more than $14,500s^{-1}$ for a high noise case during the daytime, we utilize eqn. (2.4) as the bit error rate (BER) result. And it leads to the power estimation for individual relay node in a closed form, assuming the relays maintain the same rate R_b and transmit simultaneously. Note that the delay of delivering a packet from end to end for a multihop link is N times that of direct transmission considering the time cost of decoding and forwarding at each relay node though. After some manipulations, we find the power consumption for each relay

to be

$$P_{tn} = -N^{-\alpha} \frac{R_b \xi h \nu d^{\alpha}}{\eta} \ln \left[2 - 2(1 - P_e)^{1/N} \right], \tag{2.10}$$

where P_{tn} is the transmission power for each relay node, and the distance between two consecutive relays is d/N.

Since N relays participate in the cooperative relaying, the end-to-end link has a total power consumption $P_{MH} = NP_{tn}$. Thus the overall power saving ratio, defined as $(P_{DT} - P_{MH})/P_{DT}$, can be derived using eqs. (2.8) and (2.10),

$$\Gamma = 1 - N^{1-\alpha} \frac{\ln \left[2 - 2(1 - P_e)^{1/N} \right]}{\ln(2P_e)}. \tag{2.11}$$

Note that $N = 1$ is the case of direct transmission with only source and destination nodes, and Γ becomes zero.

2.3.3 Alleviating the Directional Interference

Besides the question of how the transmit power can be reduced with the number of relays, the other issue with the NLOS multihop UV link is that each relay node sees interference from the previous relays when simultaneous transmissions are allowed to enhance the throughput. Because of the NLOS directional nature, a serial relayed NLOS UV link differs from other existing FSO communication link such as [54]. The LEDs illuminate over a NLOS geometry and the emitted optical field can also be detected by the downstream relays in addition to the immediate destination due to the scattering effect. In other words, an intermediate relay node could see the "blinking" light from more than one upstream relays. The situation is shown in Fig. 2.8.

For non-coherent detection of the intensity, the interference raises the noise level, and the quantum limited assumption no longer holds. We employ a general treat-

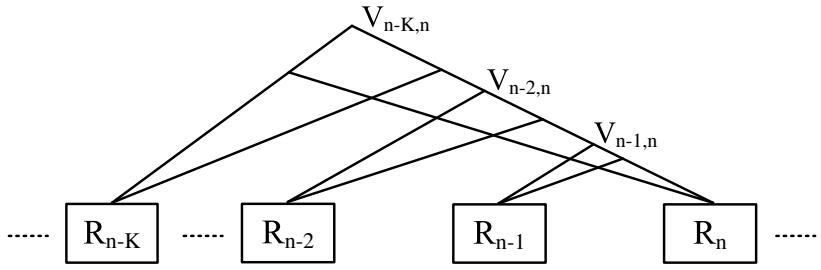

Figure 2.8: A multihop NLOS UV communication link with directional interference.

ment in the error analysis of OOK modulation to examine the performance with interference. In Fig. 2.8, the nth node can receive the signal of interest from the $(n-1)$th node and interference signals from the $(n-2)$th up to $(n-K)$th nodes assuming simultaneous transmission is permitted with no coordination. K is defined as the number of upstream interfering nodes for the $(n-1)$th node. The interfering nodes are termed upstream nodes leading the $(n-2)$th node.

Hence the average signal photon number λ_s and interference photon number λ_i during each OOK symbol interval can be expressed as

$$\lambda_s = \frac{\eta P_t}{R_b h\nu L_{n-1,n}}, \tag{2.12}$$

$$\lambda_i = \sum_{q=2}^{K+1} \frac{\eta P_t}{R_b h\nu L_{n-q,n}}. \tag{2.13}$$

where $(n-q)$ is the index of interfering relay nodes. With eqs. (2.12) and (2.13), it is instrumental to study the impact of interference from upstream relay nodes due to directional transmission and reception. The piecewise error probability for the nth hop is conditioned on the on-off symbols transmitted by the interfering nodes, given by

$$P_{en_{intrf}} = \frac{\sum Pr\left\{\hat{x}_n \neq x_{n-1} | R_{n-2}, R_{n-3}, \ldots, R_{n-K}\right\}}{2^{K-1}}. \tag{2.14}$$

The calculation has to average over all the possible interference patterns which are equally possible. Intuitively, a lower bound to eqn. (2.14) is achieved when all the

upstream nodes send "0", so the error performance is equal to that of eqn. (2.2). An upper bound is the case when "1" is transmitted from all upstream nodes. For example, consider $K = 2$ where only one interfering node sends "1". The intensity of the interference signal depends on the path loss. Since $L_{n-2,n}/L_{n-1,n} = 2^{\alpha}$, the number of interference photons during each symbol interval becomes $\lambda_i = 2^{-\alpha}\lambda_s$, which may significantly raise the noise level.

The directional interference problem arises because the relay nodes are permitted to transmit at the same time. If we arrange the transmission of each relay node in a non-overlapping time slot, it is obvious the interference is avoided at a cost of N times longer in the end-to-end delay. In this regard, we adopt spatial reuse through orthogonal time sharing that helps to minimize the directional interference and improve the throughput by a reasonable assumption that photons die out beyond a certain range and create no interference. Since we may virtually put K interfering nodes into one group and the node after every K relays may reuse the channel in terms of either time slot or frequency, K is also regarded as the spatial reuse factor. To design an effective transmission protocol, the K, N and hop length are major knobs to design. We'll assess the effects of these parameters on piecewise error performance through numerical methods.

Even though spatial reuse is employed, one has to be aware that interference may still result from the node which precedes the reuse group and transmits in the same slot position. This may deteriorate the spatial reuse performance to some extent and we thus propose a cooperative reception scheme built upon spatial reuse to fully harvest the photons from the transmissions of the nodes in the same spatial reuse group.

The mechanism is explained in Fig. 2.9. If we set the spatial reuse size to be $K = 2$, R_2 and R_3 belong to a spatial reuse group, each reserving one time slot for

transmission to their next relay. Hence R_4 is immune from the interference due to R_2's transmission when R_3 relays to R_4 in slots $T_3, T_5, T_7 \cdots$. Because the spatial reuse is arranged every K relays, the nodes S, $R_3, \cdots, R_{2n+1}$ share the same slot in time while $R_2, \cdots, R_{2n}$ reuse a different slot. Thus the interference will only be contributed from the relay node in the previous reuse group that transmits in the same time position, namely, node S. Further, consider the cooperative reception in slot T_3. Node R_4 combines the signal from R_3 and the copy previously received in T_2 from R_2. Since in an optical transceiver, the Rx and Tx are separate branches which provide the full duplex capability, R_4 is capable of both relaying and receiving in T_2. This consists in the basis for the cooperative reception. The signal and interference energy collected by R_4 for detection in this case are respectively,

$$\lambda_s = \sum_{p=1}^{K} \frac{\eta P_t}{R_b h \nu L_{n-p,n}}, \tag{2.15}$$

$$\lambda_i = \sum_{m=1}^{M} \sum_{q=mK+1}^{mK} \frac{\eta P_t}{R_b h \nu L_{n-q,n}}, \tag{2.16}$$

where M refers to the number of interfering groups leading the current spatial reuse group that transmits to node n. If $K = 2$, there are two nodes accessing the orthogonal time slots in each group.The relaying group is defined as the set of nodes that cooperate to forward the packet and interfering spatial reuse group as those preceding the relaying group in the upstream direction. Assuming there is only $M = 1$ interfering group in the analysis, for the example of $K = 2, M = 1$, eqs. (2.15) and (2.16) are expressed as

$$\lambda_s = C(1 + 2^{-\alpha}), \quad \lambda_i = C(3^{-\alpha} + 4^{-\alpha}), \tag{2.17}$$

where $C = \frac{\eta P_t}{R_b h \nu L_{n-1,n}}$.

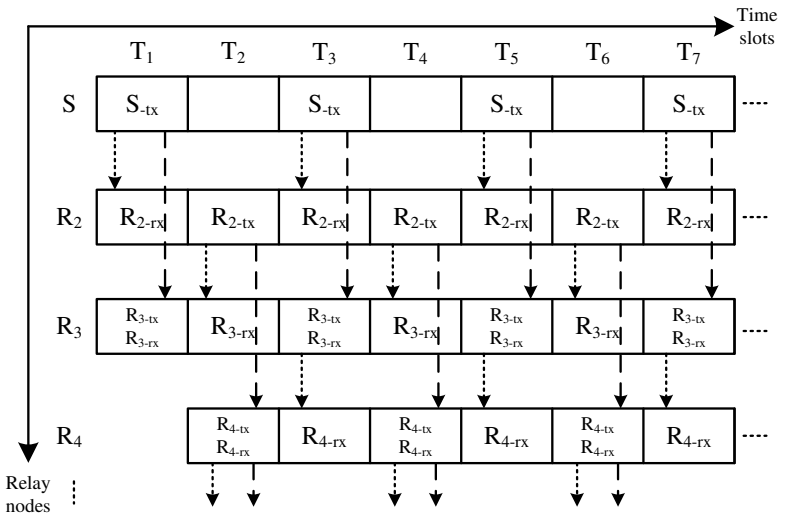

Figure 2.9: Transmission and receiving protocol for multihop NLOS UV link, $K = 2$.

2.4 Numerical Results and Discussion

This section reports the numerical studies on NLOS UV link through the scattering channel. We start with the point to point scenario and then extend the discussion to a multihop configuration. These results provide useful reference for system design. Following numerical results are depicted in Figs 2.10-2.15, which are cited from our published papers [29], [30], [33];

2.4.1 Range and Rate of Point-to-Point NLOS UV Link

We further incorporate an empirical path loss model for an NLOS UV link into bit error probability analysis for a photon counting receiver to characterize the achievable performance in terms of the baseline range and bit rate. It can be shown that the performance largely depends on the system geometry defined by pointing angles.

In Fig. 2.10, both shot noise limited case and regular background noise case

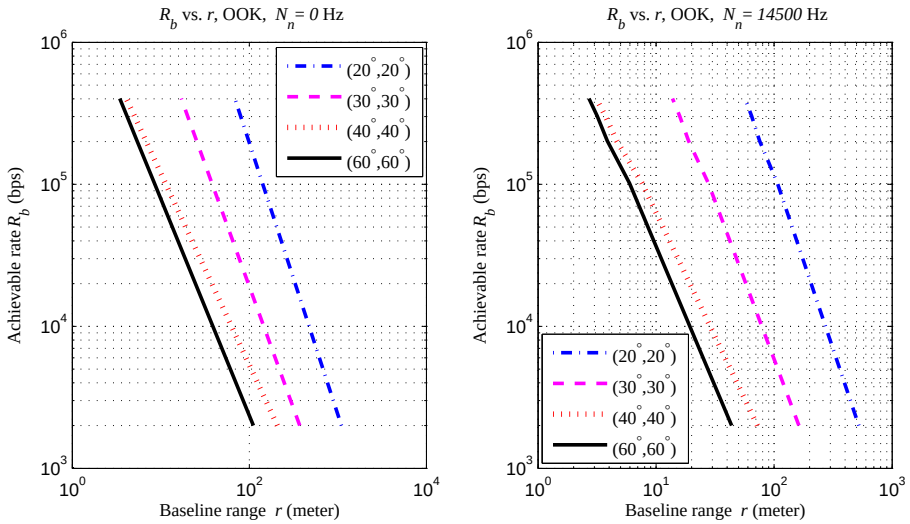

Figure 2.10: Achievable rates vs. base-line range for OOK modulation, $P_t = 50mW, P_e = 10^{-3}$, low noise (left) and high noise (right) cases.

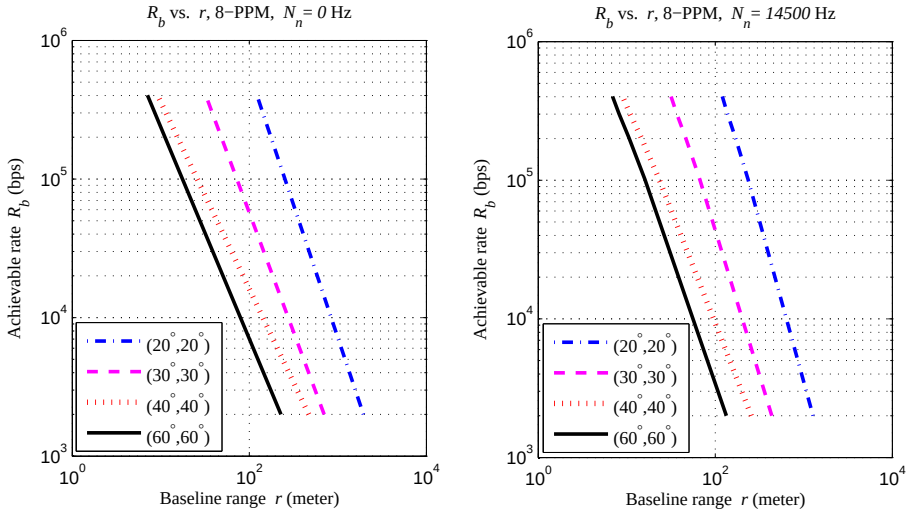

Figure 2.11: Achievable rates vs. base-line range for 8-PPM modulation, $P_t = 50mW, P_e = 10^{-3}$, low noise (left) and high noise (right) cases.

are plotted. Over the range of $100m$, with the requirement of 10^{-3} in error probability, a rate of $1k - 100kbps$ can be expected from high elevation angles to low elevation angles given $50mW$ of transmission power. When there is certain background noise due to solar radiation, achievable rate has some loss on the order of 10% less than that of shot noise limited case. By comparing Fig. 2.10 with Fig. 2.11, more than 30% increase in data rate can be boosted with higher order PPM modulation scheme. It is worthwhile to

note that since we focus on uncoded error performance, according to Shannon capacity in the perspective of information theory, extremes of range and rate shall be much higher than what we illustrate. Recently, ways to achieve the Shannon limit have been extensively and intensively studied by the coding community via graph based error control codes like LDPC codes and iterative decoding. Even without those probabilistic codes, conventional algebraic codes can be applied to improve the performance. For instance, [51] gives a Reed Solomon code based method. Interested readers are advised to read the references and therein. Our research is mainly oriented in the analysis of raw bit error rate and less touches the scope of error coding and decoding techniques.

2.4.2 Multihop NLOS UV Link Performance

In this section, we intend to prove the benefits of a serial multihop link configuration for NLOS UV communications which can save not only the power of individual relay node but also the overall power consumption of the whole link. Notice that the interference effect due to the neighboring nodes will cause higher piecewise error probability, we study the effect quantitatively. The key system parameters are summarized in Table 2.3.

As a benchmark, we first calculate the required emission power for a direct transmission NLOS link. For a quantum limited case, eqn. (2.8) is employed to predict the power. It is shown in Fig. 2.12 that Tx/Rx pointing angle pairs $(10°, 10°), (20°, 20°), (30°, 30°)$ and $(40°, 40°)$ call for emission power $15mW$, $150mW$, $1W$, and $2.5W$ over the range of $300meters$ respectively. Although the power on the order of tens of milliwatts can possibly be supplied by a LED array made of a large number of LED cores at the transmitter, the power on the order of watts at current state of the art can only provided by a UV laser, which is prohibiting in cost and cumbersome

in size.

By adopting the configuration of a multihop NLOS link, the power requirement on individual relay nodes can be relaxed by increasing the hop number. Equivalently speaking, total power is distributed to to spaced relay nodes, each of which consumes much less power. To conclude, adding more relay nodes with a fixed transmission power is an effective way to extend the range of communications. We plot in Fig. 2.13 the node power versus hop number for a multihop link at a range of $300meters$. For small angle geometry like $(10°, 10°)$ and $(20°, 20°)$, the transmitter of each node only needs one or seven LEDs to provide $10mW$ power since the effective emission power per UV LED at 250nm is around $1mW$. For large angle scenarios such as $(30°, 30°)$ and $(40°, 40°)$, $30mW$ and $150mW$ are desired for a 10-hop link over 300 meters. Such a power consumption renders possible the LED array as the light source, which is compact and lightweight. On the other hand, it is clear the overall power consumption could be saved as reflected by the power saving ratio according to eqn. (2.11). We plot it in Fig. 2.14 and find out more than 60% of power can be saved when $N > 5$ for all angles except $(40°, 40°)$ and the path loss exponent α is a determining factor. In word, it is always beneficial to get decreased individual power consumption through the use of more hops.

For the cons, we are able to identify that simultaneous transmissions of relay nodes cause interference, which largely etches the link performance. The issue can be illustrated in the link error probability in Fig. 2.15. By assuming each hop is adversely affected by the transmission of its nearest upstream hop, eqs. (2.12) and (2.13) are used to count the signal photons and interference. Then a piecewise error probability is numerically computed using eqn. (2.2) and the link error probability can be further obtained using eqn. (2.9). For a 10-hop link, without coordination of transmission, performance is demonstrated in Fig. 2.15. Interference has lowered the performance

Table 2.3: Typical parameters for UV NLOS link

Parameter	Value
Tx apex angle θ_1	$10°, 20°, 30°, 40°$
Rx apex angle θ_2	$10°, 20°, 30°, 40°$
Wavelength λ	250nm
Single LED power P_t	3mW
Information rate R_b	64kbps
Noise photon count rate N_n	14500s^{-1}
PMT efficiency η_{PMT}	30%
Optical filter efficiency η_{filter}	20%

by four orders of magnitude from 10^{-6} to 10^{-2}. This consitutes the motivation to considering a spatial reuse scheme with cooperative reception. In essence, the idea is that the separation of simultaneous neighboring transmissions shall be enlarged while cooperative reception collects more signal energy from the relay nodes in the same spatial reuse group. Eqn. (2.17) can be used to calculate the piecewise error probability in this case and we observe the link performance has been dramatically improved close to that of shot noise limited case without interference for $K = 2, M = 1$.

2.5 Summary

In this chapter, we incorporated an empirical path loss model for an NLOS UV scattered link into the bit error probability analysis by assuming an ideal model of a photon counting receiver. Since the UV channel is strongly affected by the scattering, the path loss model we considered captures such effect. Numerical methods are employed to illustrate the performance in terms of the tradeoffs of range versus rate. It is shown

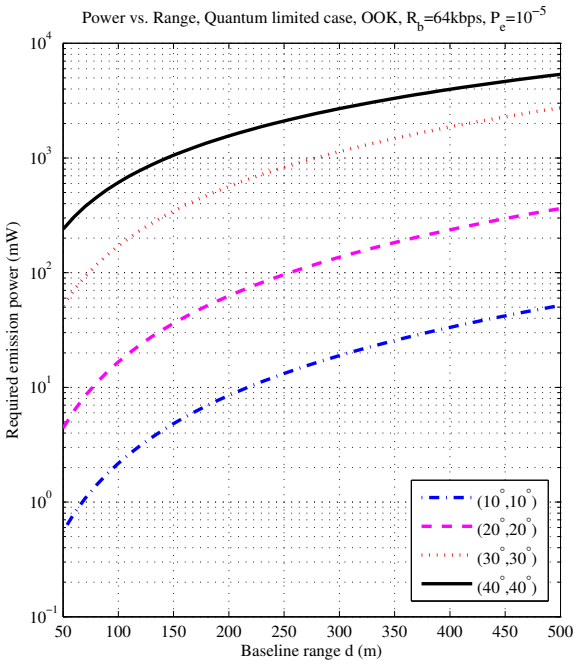

Figure 2.12: Required emission power vs. direct transmission range, quantum limited case, OOK modulation, $R_b = 64kbps$, $P_e = 10^{-5}$.

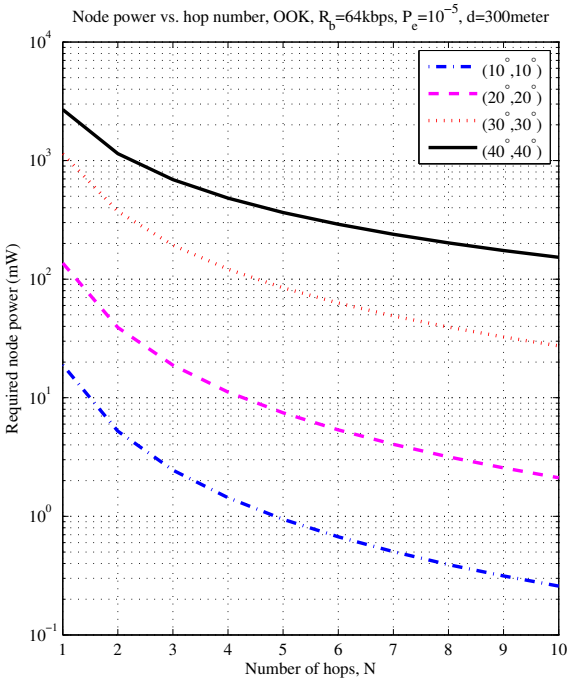

Figure 2.13: Required emission power per relay node vs. number of hops over 300 meters, quantum limited case, OOK modulation, $R_b = 64kbps$, $P_e = 10^{-5}$.

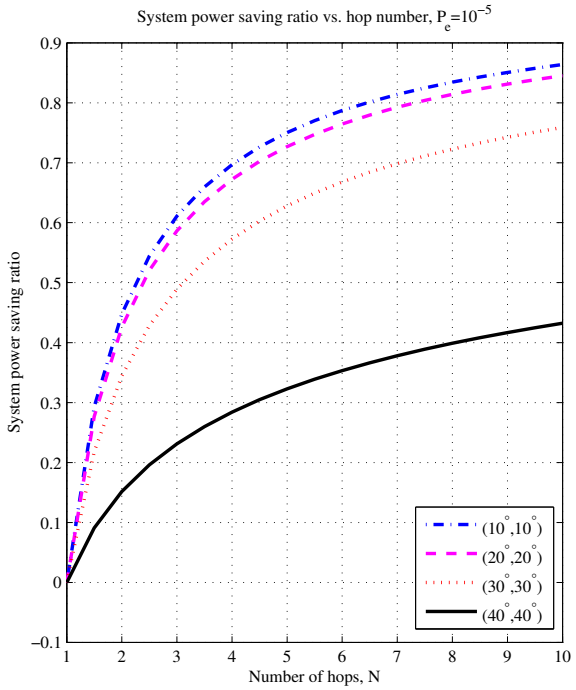

Figure 2.14: System power saving ratio with multihop link, $P_e = 10^{-5}$.

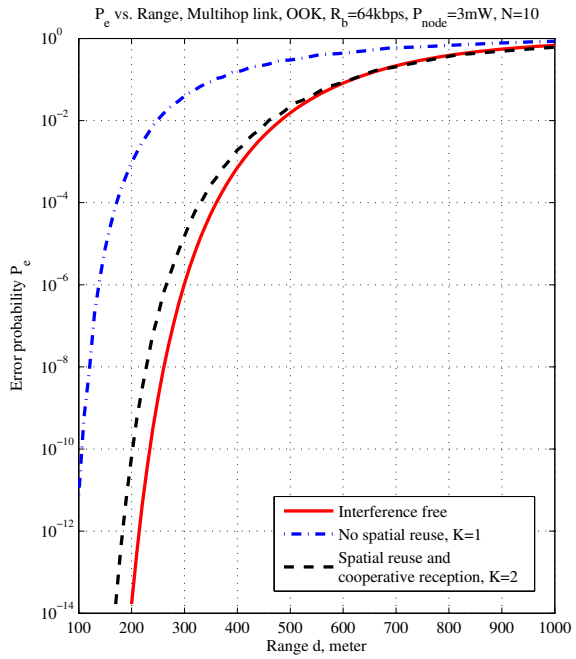

Figure 2.15: Error performance vs. range for multihop link, $(20°, 20°)$, node power $P_t = 3mW, N = 10$.

that the performance largely depends on the system geometry defined by pointing angles. These results provide useful reference for system design.

To improve the link performance and envision a feasible solution for the transmitter of NLOS UV communications, we also evaluate the power saving advantages of a multihop configuration, compared against the direct transmission. To alleviate the interference issue, we propose a cooperative reception scheme enabled by coordinated transmissions within each spatial reuse group. We show that the multihop scenario can relax the power requirement of both individual nodes and the entire system, which makes NLOS UV a viable solution for wireless sensor network.

Chapter 3

Device Dependent NLOS UV Receiver Design

Previous discussion in Chapter 2 has assumed an ideal photon counting receiver model. In practice, ideal photon counting receiver is unrealistic in the real world. We are intrigued to study the performance of an NLOS UV receiver in the presence of non-ideal photodetector and thermal noise sources. The empirical channel path loss is coupled into our model to reflect the scattering channel effect on the UV link. We introduce statistical models of common photodetectors and formulate the detection problem by modeling the random output of the photodetector. Error probability is derived for both PMT and APD involved receivers. Then, the effect of pulse broadening due to the scattering induced multi-path phenomenon is quantified into the performance model. As a building brick, we will be able to predict the capabilities of a practically achievable UV receiver eventually.

In Section 3.1, the structure of an optical receiver is presented and the randomness in photodetector is elaborated. We develop the performance models for two

typical photodetector based receivers by incorporating their statistical models. Since direct counting on secondary photon-electrons might incur a large computation burden, a simpler model utilizing the knowledge on the primary photon arrival rate is proposed in Section 3.2 on top of which the receiver performance is obtained in Section 3.3. Section 3.4 further extends the scope of study by quantitative evaluation on the influence of ISI unique to the scattering channel. Numerical results and discussions are presented in Section 3.5.

3.1 Introduction

We take a closer look at the NLOS UV communication system in this chapter. An abstraction on the NLOS UV communication system is given in Fig. 3.1. The UV LED array is driven by the modulator at the transmitter while the receiver can be either PMT or APD combined with a solar-blind optical filter. The output of the photodetector is connected to the post-processing circuit, consisted of an integrator and an detection unit on the decision path. The receiver shall also include a clock recovery module which will not be covered in our discussion.

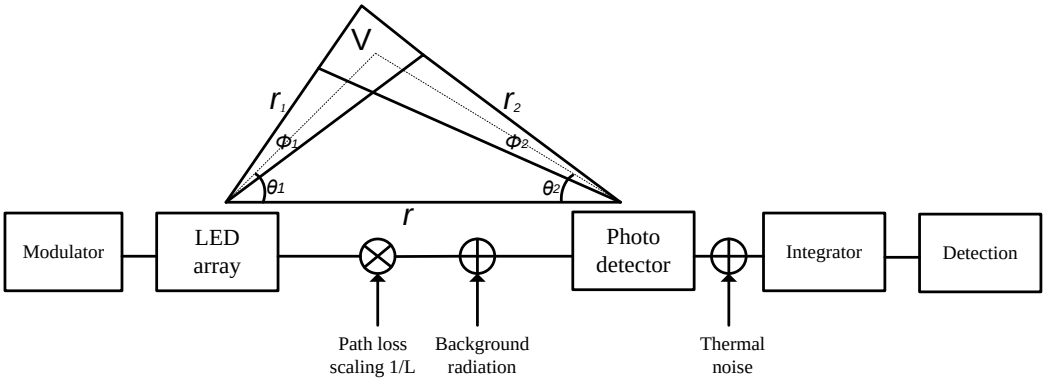

Figure 3.1: A NLOS UV communication system model.

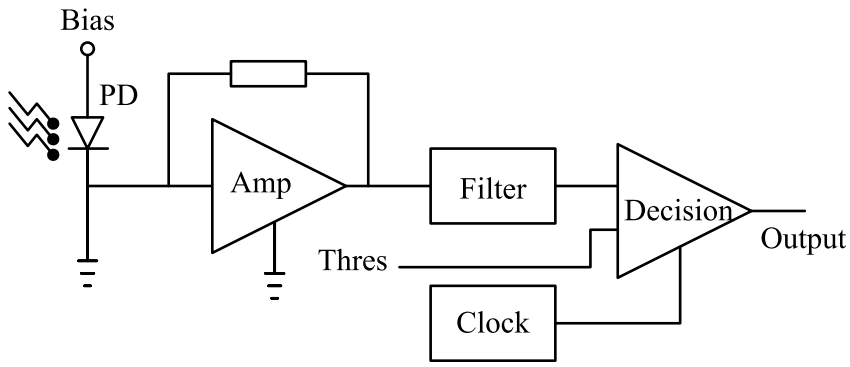

Figure 3.2: A NLOS UV receiver.

Specifically, the electronic circuit of an NLOS UV receiver is depicted in Fig. 3.2. Between the photodetector and the decision circuit lies a low noise transimpedance amplifier to convert the current signal into voltage signal. Take the instance of OOK, a receiver has a decision unit which is threshold based. When the waveform out of the integrator is higher than the threshold, one is determined; otherwise, zero is produced.

Several sources in the whole communication link hinder the ultimate performance. Firstly, the scattering channel enormously attenuates the optical power arrived at the receiver. For the purpose of link budget, the loss of power must be accurately estimated and certain margin shall be added, which relies on the effectiveness of the path loss modeling. Secondly, the background radiation introduces additional optical noise overlapping to the signal. In the worst case, it might cause saturation to the optical front end of the receiver. For NLOS UV communications, this can be less of a concern due to the low level of solar noise and the employment of highly selective optical filter. Aided by orthogonal modulation scheme such as PPM, the influence of background noise may be further minimized owing to the detection method.

However, besides channel attenuation, there is also randomness in the photomultiplication process of the photodetector. The randomness in part results from the

nature of the statistical interaction between the radiation optical field and the released electrons of the photosensitive material. We learned from section 1.2.2 that through the treatment of quantum theory, the theoretical analysis shows the emitted number of electrons k by the photodetector has a probability following the Poisson distribution with the mean m_ν,

$$Pr\{k\} = \frac{m_\nu^k e^{-m_\nu}}{k!}, \tag{3.1}$$

where m_μ depends on the integral of incoming optical intensity over a short period of time. Eqn. (3.1) justifies the handling of performance analysis in the Poisson communication regime.

A unique issue exists with the type of photodetector that has the amplification gain which allows the primary photoelectrons (k_1) to be boosted into a larger quantity of secondary photoelectrons (k_2). The randomness in the gain of the photodetector will cause the variation of the statistics of the output count, deviated from the Poisson distribution. In consequence, we may not directly foot on the assumption of a Poisson counting receiver to derive the analysis.

Last but not the least, the receiver electronics circuit produces thermal noise which behaves like additive white Gaussian noise (AWGN). The signal is thus further complicated by the noise and the statistics of the output to be handled by the decision unit has to be modeled with care by considering aforementioned factors from optical domain into electronic domain, from photodetector to post processing circuits.

Our mission is to develop a statistical model of the signal output and characterize the link level error performance.

3.2 Statistical Modeling of Photodetector Output

3.2.1 Conditional Probability Distributions of PMT/APD

To capture the random gain effect of the photodector, it is obvious one has to characterize how the secondary photoelectrons depend on the primary photoelectrons statistically described by the conditional probability distribution $P_{k_2|k_1}(k_2|k_1)$. The number k_2 of the secondary photoelectrons shall conform with a probability mass function that has the form,

$$P_{k_2}(k_2) = \sum_{k_1=0}^{\infty} P_{k_2|k_1}(k_2|k_1) P_{k_1}(k_1), \tag{3.2}$$

where $P_{k_1}(k_1)$ is the primary photonelectron probability described by eqn. (3.1) and $P_{k_2|k_1}(k_2|k_1)$ is the conditional probability of secondary photoelectrons depending on k_1. There has been a rich amount of literature since 1960s on modeling $P_{k_2}(k_2)$ for the photodetectors, namely, PMT and APD types. The important part of the modeling work is to determine appropriate conditional probability of k_2 given k_1, which reflects the photodetectors' amplification process. In practice, direct analysis based on eqn. (3.2) demands high complexity in numerical calculation involving a huge number of summations so as to cover the range of secondary PEs. Alternatively we resort to the models that directly describe the probability of k_2.

It is proposed for PMT, the probability of PMT's secondary photoelectrons is

$$P_{k_2}(k_2) = C \exp\left[\frac{-(k_2 - A\lambda)^2}{2(\zeta A\lambda)^2}\right], \tag{3.3}$$

where C is the normalization factor, λ is the average arrival rate of the primary photoelectrons and ζ is the spreading factor of PMT which is the variance of PMT's random gain A. Then the excess noise factor F which is the ratio of the mean squared gain to the square mean and has the form $F = 1 + \zeta^2$. While for the APD case, we follow the

model shown by McIntyre and Conradi [18], [47] as

$$P_{k_2}(k_2) = \frac{1}{(2\pi C_1^2)^{1/2}} \left[\frac{1}{1 + \frac{(k_2 - A\lambda)^{3/2}}{C_1 C_2}} \right] \exp\left(\frac{-(k_2 - A\lambda)^2}{2C_1^2 \left[1 + \frac{(k_2 - A\lambda)^2}{C_1 C_2}\right]} \right), \tag{3.4}$$

where

$$\begin{aligned} C_1 =& (A\lambda)^2 F - 1 \\ C_2 =& A(\lambda F)^{1/2}/(F-1) \\ F =& \gamma A + (2 - \frac{1}{A})(1-\gamma). \end{aligned}$$

F is the excess noise factor jointly determined by the ionization factor γ and gain A. With the typical values of $\zeta = 0.1$ and $gamma = 0.028$, F takes the values 1.01 and 4.7343 for a PMT and APD (with gain 100), respectively. It is true that we may rely on the statistics of the number k_2 of the secondary photoelectrons to investigate the performance of detection considering the modulation scheme in a classic way. Nevertheless when the photodetector is embedded as part of the receiver with post processing electronics, thermal noise comes into the plate, which should not be ignored. We are thus motivated to further study the output statistics by incorporating the thermal noise in the next section.

3.2.2 Modeling Photodetector Output in the Presence of AWGN

Fundamentally, electronic noise is additive to the desired signal and the decision variable for detection of s from z takes the form

$$z = s + n \tag{3.5}$$

where n is the thermal noise which is a normal random variable and s is the output current of the photodetector. As a Gaussian random variable, n has the variance given

by

$$\sigma_n^2 = (2k_e T^o / R_L) T_p, \tag{3.6}$$

where k_e, T^o and R_L denote the Boltzmann constant, the receiver temperature (Kelvin), and the load resistance. T_p is the slot interval for pulse-based modulation such as OOK and PPM assuming non-return-to-zero pulse. Clearly the eqn. (3.6) indicates the dependence of noise effect on transimpedance amplifier with which the photocurrent is converted to voltage signal and the operation temperature.

Consider the additional relationship of photoelectric signal s and the zero mean AWGN n, the noise shall have a non-zero mean due to the output of photodetector when the secondary photoelectrons has a number of k_2. Thus

$$\mu = k_2 e. \tag{3.7}$$

Conditioned on the average count λ of primary photoelectrons per pulse, the conditional probability density of z being $p_z(z|\lambda)$ is an average of the continuous Gaussian distribution over the discrete probability of the secondary photoelectrons as below

$$p_z(z|\lambda) = \sum_{j=0}^{\infty} P_{k_2}(k_2 = j|\lambda) G(z, je, \sigma_n^2). \tag{3.8}$$

In eqn. (3.8), $G(z, a, b)$ denotes the probability distribution as a Gaussian random variable z with the mean a and the variance b. $P_{k_2}(k_2 = j)$ has to take the form as in eqn. (3.3) for the case of PMT and eqn. (3.4) for APD.

A drawback in the application of eqs. (3.7) and (3.8) to obtain a numerical solution is that a large quantity of computations are required to cover the range of secondary PMT photoelectrons. For example, since the photoelectron output of a high gain PMT can be on the order of 10^5 to 10^8, the accumulation process has a correspondingly prohibitive computational burden. As an alternative, we choose to directly

model the random gain effect with the thermal noise, as proposed in [40]. The approach assumes every arrival of a primary photoelectron stimulates multiple secondary PEs in the number of roughly $A_i e$, where A_i is the realization of random gain accompanying each amplification process triggered by the primary PEs. And z can be expressed as

$$z = s + n = \sum_{i=1}^{k_1} A_i e + n. \tag{3.9}$$

From time to time, the gain of the photodetector A_i is independent but Gaussian distributed with the average Ae where A is the mean of the gain. The variance is defined through the excess noise factor F as $(F-1)(Ae)^2$. Now it is interesting to find the distribution of z as a summation of multiple Gaussian random variables as

$$p_z(z|\lambda) = \sum_{j=0}^{\infty} P_{k_1}(k_1 = j|\lambda) G(z, jAe, \sigma^2), \tag{3.10}$$

where $P_{k1}(k_1 = j)$ assumes the form of eqn. (3.1), and σ^2 involves the contributions from both the thermal noise and the random gain effect of the photodetector

$$\sigma^2 = \sigma_{PD}^2 + \sigma_n^2, \tag{3.11}$$

$$= (F-1)(Ae)^2 + (2k_e T^o / R_L) T_p. \tag{3.12}$$

By substituting the expressions of excess noise factor F for PMT and APD respectively, eqn. (3.11) may be rewritten as

$$\sigma_{PMT}^2 = j(\eta Ae)^2 + (2k_e T^o / R_L) T_p, \tag{3.13}$$

$$\sigma_{APD}^2 = j[\gamma A + 2(1-\gamma) - \frac{1-\gamma}{A} - 1](Ae)^2 + (2k_e T^o / R_L) T_p \tag{3.14}$$

To this end, the distribution of z can be determined with much less number of summations in the range of primary PE number k_1 compared with the approach in eqn. (3.8).

3.3 Performance of NLOS UV Receiver with Amplifier

Aided by the statistics and the path loss model from the previous sections, we are now ready to evaluate the error performance, rates, and ranges that can be achieved by a short range NLOS UV communication system.

3.3.1 Optimal Decision of OOK for Non-ideal Receiver

For OOK modulation, the receiver adopts the threshold-based direct detection, and a more general expression of error probability can be expressed as below which is an application of the results of OOK given in section 2.1.3. The error probability can be written as

$$\begin{aligned} P_{e_{OOK}} =& P_1 Pr\{z < z_{th}\} + P_0 Pr\{z >= z_{th}\} \\ =& P_1 \int_{-\infty}^{z_{th}} p_z(z|\lambda_s + \lambda_b)dz + P_0 \int_{z_{th}}^{\infty} p_z(z|\lambda_b)dz, \end{aligned} \tag{3.15}$$

where P_1 and P_0 are the probabilities of source transmitting 1 and 0, respectively. We assume $P_1 = P_0 = 0.5$. Without any constraint, the threshold can be obtained through the minimization of $P_{e_{OOK}}$, which is achieved by specifying the derivative of $P_{e_{OOK}}$ with respect to z_{th} equal to zero. That is

$$\frac{dP_{e_{OOK}}}{dz_{th}} = 0. \tag{3.16}$$

And we have

$$p_z(z_{th}|\lambda_s + \lambda_b) = p_z(z_{th}|\lambda_b). \tag{3.17}$$

Given the general form of pdf of z in eqn. (3.10), an equation for the optimal z_{th} shall be a mixture involving both summations and integral, which prohibits the development of close form representation. Hence we seek a numerical approach instead.

Using eqn. (3.10) for $p_z(z)$ and applying the following identity, we shall first determine z_{th} numerically.

$$\int_{-\infty}^{z_{th}} p_z(z|\lambda_s + \lambda_b)dz = 1 - \int_{z_{th}}^{\infty} p_z(z|\lambda_s + \lambda_b)dz. \tag{3.18}$$

In the second step, eqn. (3.15) can be found in a more compact form lending itself to an easier numerical solution by noticing the fact that Q-function is involved.

$$P_{e_{OOK}} = \frac{1}{2} - \frac{1}{2}\sum_{j=0}^{\infty}\left[\frac{(\lambda_s+\lambda_b)^j}{j!}e^{-(\lambda_s+\lambda_b)} - \frac{\lambda_b^j}{j!}e^{-\lambda_b}\right]Q\left(\frac{z_{th}-jAe}{\sigma}\right). \tag{3.19}$$

3.3.2 Performance of PPM Demodulation

M-ary pulse position modulation (M-PPM) is widely employed as a pulse-based modulation option, where the receiver is based on the maximum likelihood method by comparing the outputs of different slot positions without a need for the threshold. A general form of the error probability of PPM demodulation has been given in eqn. (2.7). In our context of the background noise, thermal noise and photodetector's random gain effect, the correct detection probability has to be rewritten as

$$\begin{aligned} P_{e_{PPM}} =& \frac{1}{2^M-1}\sum_{j=0}^{\infty}\frac{(\lambda_s+\lambda_b)^j}{j!}e^{-(\lambda_s+\lambda_b)} \\ & \int_{-\infty}^{\infty} G(z, jAe, \sigma^2)\left[1+\sum_{k=0}^{\infty}\frac{\lambda_b^k}{k!}e^{-\lambda_b}erf\Big(\frac{z-kAe}{\sqrt{2}\sigma}\Big)\right]^{M-1}dz, \end{aligned} \tag{3.20}$$

where $erf(x)$ is the error function as

$$erf(x) = \frac{2}{\sqrt{\pi}}\int_0^x e^{-u^2}du. \tag{3.21}$$

Now that we have derived the performance equations, numerical results will be presented in Section 3.5.

3.4 PMT Based Receiver under ISI Effect

3.4.1 Scattering Induced Pulse Broadening

In Section 2.1.2, it is reported the scattering channel not only tremendously attenuates the light signal but also broadens the light pulse because of the multiple paths of propagation caused by the numerous scatterers in the atmosphere. For higher speed communication over the NLOS UV link, since mostly pulse based modulation schemes are employed, the pulse broadening will result in the inter-symbol-interference (ISI) undoubtedly.

The authors of [17] present measurement results from several scenarios by varying the optical pointing and receiver field of view (FOV). Such measurement requires the emission of a ultra short UV pulse which has to rely on the UV laser as the source. Constructed channel sounding platform is depicted in Fig. 3.3. The narrow beam angle of the laser beam needs to be widened with an optical lens. The measurements show the pulse broadening as a function of receiver (Rx) and transmitter (Tx) elevation angles, receiver FOV, beam angle, and Tx-Rx separation distance.

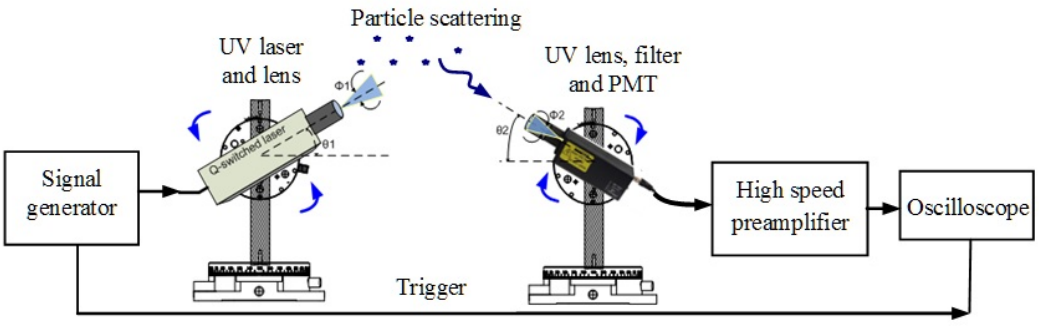

Figure 3.3: A UV Laser based channel sounding platform [17].

Although a comprehensive model on pulse delay spread has not been provided

even with the availability of preliminary measurement results, we intend to predict the potential performance loss on the NLOS UV link due to ISI. In literature of UV communications, this has not been studied before. In our analysis, a PMT based receiver is assumed and results from last section are further extended to take into account the interference. To evaluate, we propose a way to quantify the contribution from broadened pulse into current symbol of interests in the time domain.

3.4.2 Evaluation on ISI Effect

Our derivation on the NLOS UV receiver under the ISI effect due to the scattering channel follows the same framework of above section and quantifies the influence of pulse broadening on the detection process. An extra portion of energy in the number of interfering photons is introduced into the problem formulation.

To start with, a linear time invariant (LTI) model of the scattering channel is the premise. Intuitively, the experimental measurements on the channel impulse response indicate certain stationarity. It is reasonable since the optical receiver is not a mobile terminal, Doppler effect is limited which justifies the very slow changing nature of the channel characteristics. During the measurement campaign, it was observed the channel response needed an averaging of $20 - 50$ Hz to appear a steady shape. Thus the correlation time T_c shall be within $20 - 50ms$ which is much longer than the symbol period of the typical rates in the application scenarios that are considered. In these applications, OOK symbol durations are on the order of $1us - 1ms$. This means tens of thousands of OOK symbols share the same correlation time span, during which the channel is viewed as a stationary LTI system.

With a pulse modulation scheme, the channel input is a non-return-to-zero pulse during one of the slot T_s in each symbol time T_s. MPPM requires $T_s = MT_p$.

Define T_h to be the time length of the channel impulse response and the duration of the received light pulse out of the channel is extended to $T_p + T_h$ and it will thus has a tail part infiltrating the neighboring slot in the same symbol or even spanning multiple symbols. Quantitatively, the total number of slots covered by the received pulse after channel broadening is

$$N_{slot} = \left\lceil \frac{T_p + T_h}{T_p} \right\rceil. \tag{3.22}$$

We further define $Nsymbol$ as the number of preceding symbols affecting the present symbol,

$$N_{sym} = \left\lceil \frac{T_p + T_h}{T_s} - 1 \right\rceil. \tag{3.23}$$

where $N_{slot} = MN_{sym} + 1$.

To determine the pulse shape of received signal, the transmitted pulse is assumed to take the rectangular shape $p(t)$ without any loss of generality. The channel impulse response is measured to be $h(t)$. Then the received waveform of the light can be numerically obtained through the convolution as $y(t) = p(t) \otimes h(t)$. By equally partitioning the received waveform into slots with the length of T_p, a vector $\mathbf{K}$ of multiple slots is readily available, characterizing the distribution of energy in each slot in terms of the number of photons.

$$\mathbf{K} = [K_1, K_2, ..., K_{MN_{sym}+1}]. \tag{3.24}$$

Because of the ISI, previous symbols could cause energy leakage into a current slot. We

introduce extra components in the eqn. (3.20) which represent the effect of ISI terms

$$
\begin{aligned}
P_{e_{PPM}} =& \frac{M}{2(M-1)}\left\{1-\int_0^{\infty} p(\nu_1|1,I_{D0})\left[\int_0^{\nu_1} p(\nu_2|0,I_g)\nu_2\right]^{M-1} d\nu_1\right\}, \\
=& \frac{1}{2^M-1}\sum_{j=0}^{\infty}\frac{(\lambda_s+\lambda_b+I_{D0})^j}{j!}e^{-(\lambda_s+\lambda_b+I_{D0})} \\
& \int_{-\infty}^{\infty} G(z,jAe,\sigma^2)\left[1+\sum_{k=0}^{\infty}\frac{(\lambda_b+I_g)^k}{k!}e^{-(\lambda_b+I_g)}erf\Big(\frac{z-kAe}{\sqrt{2}\sigma}\Big)\right]^{M-1} dz, \quad (3.25)
\end{aligned}
$$

where λ_s and $I_g(g=1,2,,M)$ are the transmitted photon counts in the signal slot and the accumulated ISI in the g-th slot of the present symbol of interests. Especially when $g=D_0$, $I_g=I_{D_0}$ is the contribution of the ISI to the signal slot. λ_b is the count of background noise photons during each slot of length T_p. D_0 indicates the slot position that contains the signal in the present symbol and depends on the information that is modulated. D_0 takes any value in the set $\{1,2,,M\}$. λ_s and I_g can be summarized in the following equations,

$$\lambda_s = K_1; \quad (3.26)$$

$$
I_g = \begin{cases} \sum_{i=1}^{N_{sym}+1} K_{iM-D_i+1+g}, & g \le D_0 \\ K_{g-D_0+1}+\sum_{i=1}^{N_{sym}+1} K_{iM-D_i+1+g}, & Otherwise, \end{cases} \quad (3.27)
$$

where index i is the symbol index whose range is $\{0,1,,Nsymbol\}$. Di represents the position of the signal slot in a preceding symbol with $i=1$ and $i=Nsymbol$ corresponding to the nearest and farthest symbol respectively. I_g is a piecewise function because the slots preceding the signal slot within the same symbol can not be affected by it in a causal way. Thus when g is less than D_0 the ISI in the gth slot is only composed of the interference from the previous $Nsym$ symbols.

We illustrate in Fig. (3.4) how above quantities connect to each other and result in the performance degradation. Essentially, the ISI could come from any preceding

symbols when their tails extend into the slot of interest in the current symbol to be detected.

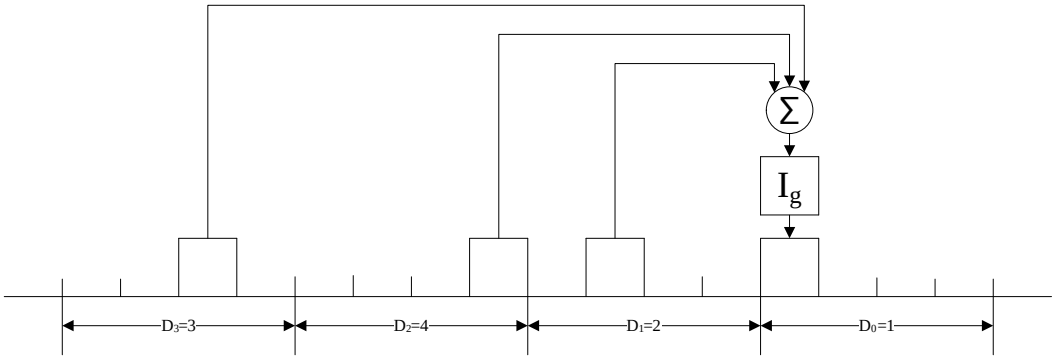

Figure 3.4: ISI contributes to current symbol of interests.

3.5 Numerical Results and Discussion

We report in the section three major contributions to the knowledge of the scattering effected NLOS UV link performance. By considering both device models and thermal noise specific to the electronics of the receiver, the prediction on achievable performance of raw BER is summarized firstly. Further noticing the fact that the noise effect is relevant to the amplifier gain settings, it is shown the gain control may be optimized in terms of the overall BER. An extension to the photodetector based receiver of NLOS UV lies in the evaluation on ISI which is resulted from the pulse broadening. The numerical analysis in this case is presented lastly.

All figures below are cited from our published works [34],[67].

3.5.1 Evaluation on PMT/APD Based UV Link

In view of the variations in link path loss under different system configurations, we are intrigued in the performance achieved by NLOS UV communication. The NLOS UV channel path loss features a huge dynamic range up to 100dB from small to large pointing angles, which necessitates the receiver capable of handling the weak optical signal and minimizing the random noise effect. We propose to rely on the highly sensitive PMT/APD in the deep UV range and concatenate with a trans-impedance amplifier to maintain a low noise operating condition. When the data rate is adequately below 10Mbps, we neglect the mild limitation from the channel frequency response, although pulse-broadening induced bandwidth limitation is an important detrimental factor under extensive experimental testing whose results will be reported elsewhere once available. Thus a NLOS UV channel is assumed mainly path loss limited for mid-to-high pointing angles. For low pointing angles, the channel has more capacity to offer large bandwidth and an equalizer can always be introduced to improve the bandwidth of high impedance amplifier [5] even in the absence of channel induced inter-symbol interference. Given typical system parameters as listed in the Table 3.1, the numerical analysis covers several aspects in the evaluation of performance.

The error performance of photodetector with background and thermal noise is demonstrated in Figs. 3.5 and 3.6 according to eqs. (18) and (20). We pick several typical data rates to facilitate the comparison with fixed PMT/APD gain and transmit power. Large-angle setups of the NLOS UV channel render huge path loss and weak signal power. A high gain photodetector is necessary to enhance the detection by post-processing circuits and satisfy the requirement of error performance. For the numerical analysis, we set PMT and APD gains at 10^4 and 250 respectively and assume the APD

Table 3.1: Typical parameters for UV NLOS link

Parameter	Value
Tx apex angle θ_1	$10°, 20°, 30°, 40°$
Rx apex angle θ_2	$10°, 20°, 30°, 40°$
Tx average power P_t	100mW
Noise photon count rate N_n	14500s^{-1}
Optical filter transmission η_f	20%
PMT efficiency η_{PMT}	30%
PMT spreading factor ζ	0.1
APD ionization factor γ	0.028
Load resistance R_L	$5M\Omega$
Operating temperature	300K

has the same detection area and quantum efficiency as the PMT does.

Let's first compare the PMT receiver and APD receiver assuming threshold based detection for OOK modulation in Fig. 3.5. PMT receiver with high gain excels in achieving higher data rate or better error performances with all four setups. The APD receiver performs much worse than the PMT since only the $(10°, 10°)$ case can barely reach the 10^{-3} error probability at 70 meters. We comment it is related to the excess noise due to the APD gain that raises the error floor and its limited multiplication capability. More analysis will be given in the next sub-section.

More power efficient modulation like 4-PPM is taken into account in Fig. 3.6. The typical data rates at the range of 60 meters yield the error performance well below 10^{-3} for most setups. The improvement on the increased data rate is obvious when compared with the OOK modulation for both PMT and APD receivers. A cross-comparison between PMT and APD in Fig. 3.5 and Fig. 3.6 also validates PMT as an effective solution to provide a viable communication link of large angle setups.

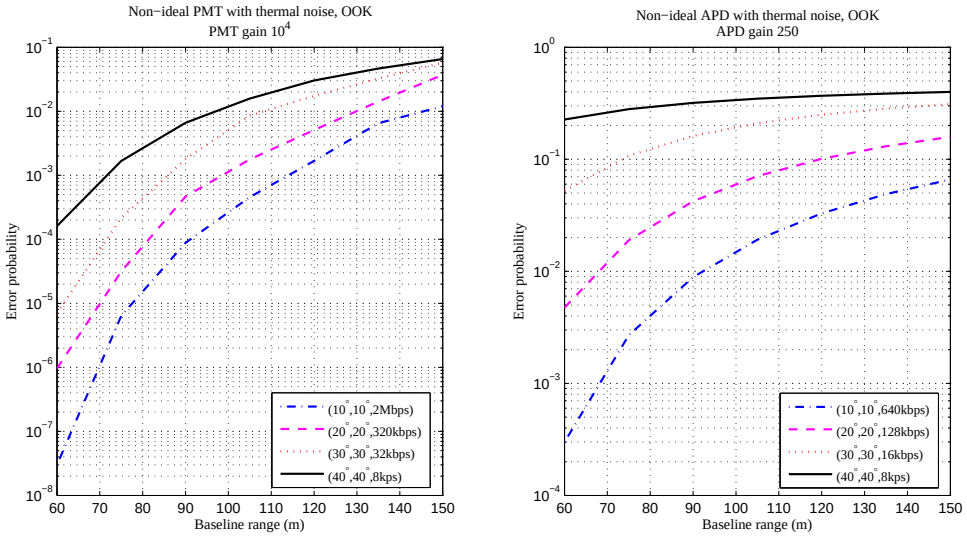

Figure 3.5: Error probability vs. baseline range for OOK modulation, $Pt = 100mW$, PMT (left) and APD (right).

3.5.2 Optimization on Detector Gain Control

Although the NLOS UV channel features a large variation of path loss related to system configuration, our analysis so far has assumed fixed gain of the detector. Since both PMT and APD amplification gains can be controlled through the bias voltage, we intend to take a close inspection of the gain effect on the performance. Intuitively, because of the non-ideal nature of the amplification process, excess noise is dependent on signal level and gain variance. A simple increase of gain may not be a panacea in all circumstances

With Fig. 3.7, we can identify performance differences between PMT and APD receivers at the range of 50 meters. For PMT, the error probability improves monotonically with increased gain, but becomes saturated when gain exceeds about 10^4. The extent of improvements differs with pointing setups, the larger the smaller pointing angles. Also for very large gain, the error performance is significantly better at small angles. For APD, error probability first decreases as gain increases and then

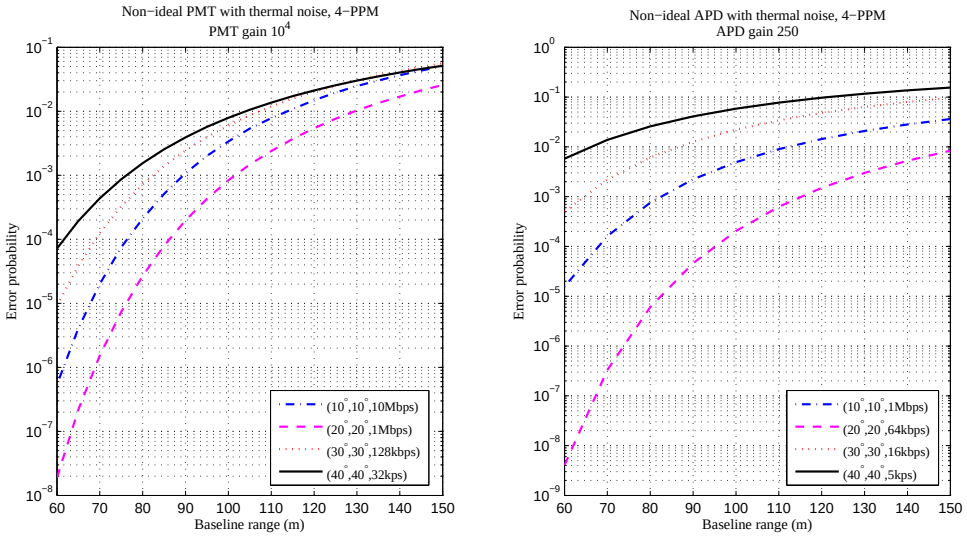

Figure 3.6: Error probability vs. baseline range for 4-PPM modulation $Pt = 100mW$, PMT (left) and APD (right).

increases after certain point. The variation is more pronounced for small pointing angles than large ones. This observation suggests that an optimal gain exits in each geometric setup. That optimal point tends to shift to a large value as pointing angle increases. The optimal gain is around 150 for $(10^o, 10^o)$ pointing case and becomes 300 for $(40^o, 40^o)$ pointing case. In comparison, PMT shows much better detection performance than APD. A high gain PMT based receiver is practically feasible for all angle setups of the NLOS UV communication system. For APD oriented receiver, excess noise from random gain fluctuation significantly degrades performance, and an automatic gain control mechanism shall be incorporated to adjust the APD bias voltage.

3.5.3 NLOS UV link under ISI Effect

We next investigate four typical scenarios from small pointing angles to relatively large ones to illustrate the effect of ISI. Due to the experimentation limitations, the pulse broadening results are based on the laser transmitter at $266nm$ while the path loss measurements are based on LEDs at $259nm$. We assume that a UV channel in these

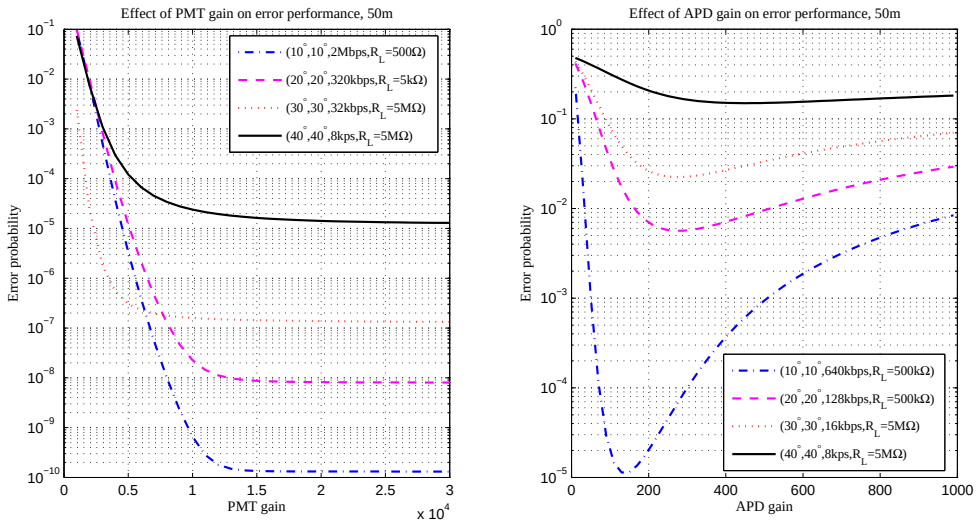

Figure 3.7: Error probability vs. multiplication gain, Pt=100mW, PMT (left) and APD (right).

two wavelengths excited by two different sources (coherent versus noncoherent) behaves in a similar fashion. Revelant theoretical study and experimental validation constitute an open research area.

Fig. 3.8 shows the numerical results for a 4-PPM receiver in four different transmit/receive pointing angles at distance of $100m$. In the geometry with both θ_1 and θ_2, equal to 10^o (Fig. 3.8(a)), BER of 10^{-3} has its support if data rate is lower than $4Mbps$. Fig. 3.8(b) shows that the data rate is confined within $500kbps$ to attain a BER lower than 10^{-3} at the elevation angles of $(20°, 20°)$.

If the same level of requirement on BER is insisted, possible data rate drops to $40kbps$ in the case of $(\theta_1, \theta_2) = (30^o, 30^o)$ and to $9kbps$ when $(\theta_1, \theta_2) = (40^o, 40^o)$, respectively. The author would like to bring to the readers' awareness advanced coding schemes and receiver techniques have not yet been applied to the system, thus the data rate mentioned above is raw data rate which is possible to be increased to a much higher order. When pointing angles are increased, the performance with and without

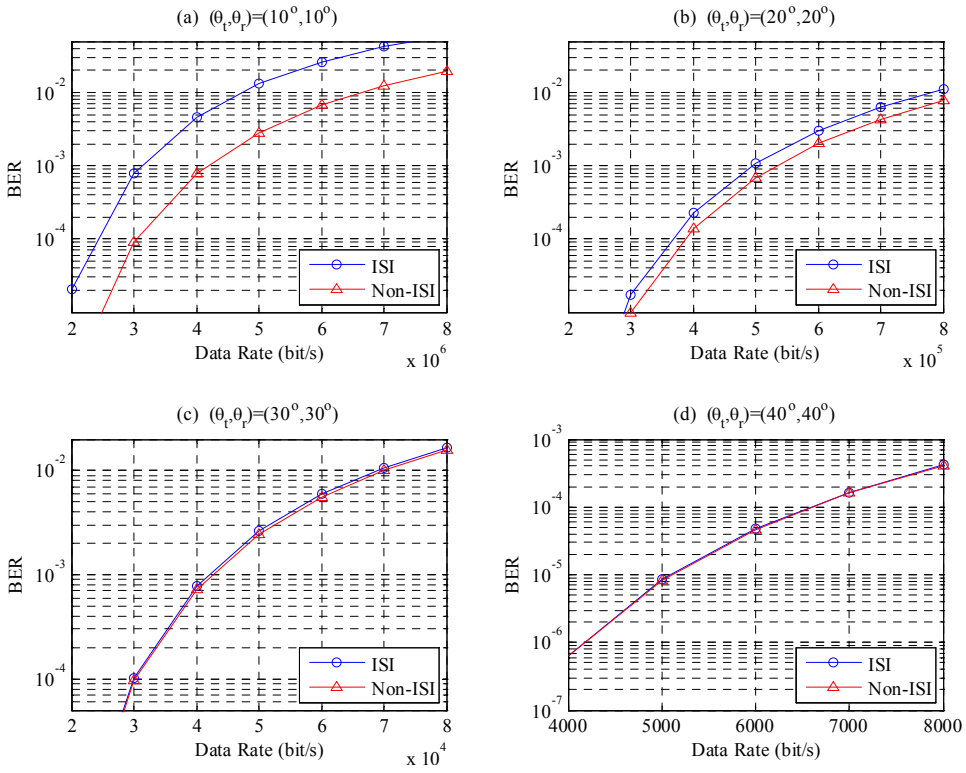

Figure 3.8: BER performance of 4-PPM receiver in ISI NLOS UV channel.

the consideration of ISI effect trends to converge, which is because the path loss effect becomes dominant in large pointing angle geometry, i.e., power loss is the main limiting factor rather than channel bandwidth. Thus under certain geometry the impact of power loss could overwhelm that induced by ISI. Another reason is that the data rate we focus on in the large pointing angle scenario is much lower than that in small pointing angle case in order to obtain meaningful BER (such as lower than 10^{-1}). Therefore, in the power limited regime, ISI effect does not appear much impacting on the performance.

The power penalty caused by the ISI effect is shown in Fig. 3.9. The power penalty is defined as $P_{penalty} = (P_{ISI} - P_{NONISI})/P_{NONISI}$, where P_{ISI} and P_{NONISI} are the power requirements with the same BER performance with and without considering channel broadening, respectively. As expected, the power penalty increases with

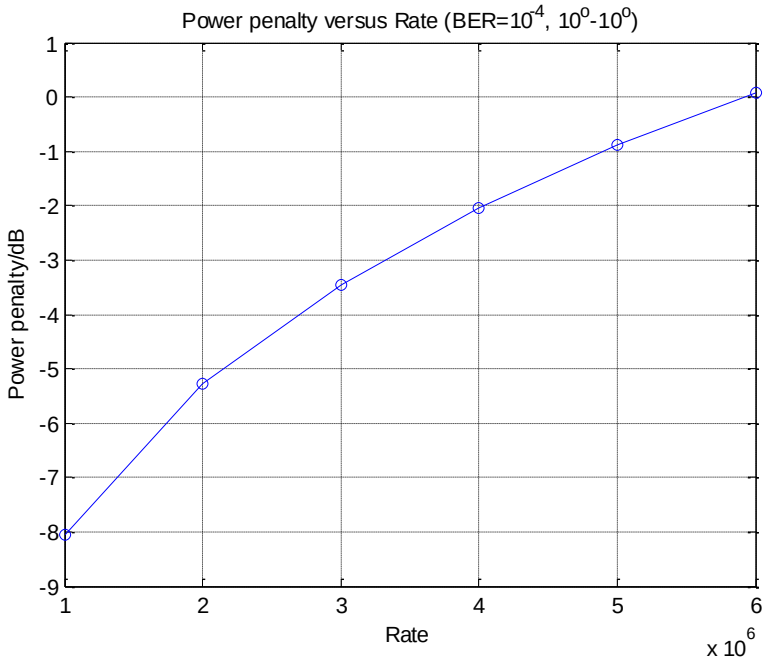

Figure 3.9: Power penalty versus data rate in UV channel with 4-PPM employed.

the increased data rate.

3.6 Summary

In this chapter, we investigated the PMT and APD based receiver performance for NLOS UV communications which is a more realistic scenario. The tradeoffs of data rate, range and error performance are presented by combining the empirical path loss model of the NLOS UV scattering channel. The effects of both photodetectors' random gain, thermal noise and background noise are comprehensively revealed utilizing the statistical model we proposed. The principles in the gain control of PMT and APD are illustrated to assist the actual system design. The results and conclusions are valuable through the application of channel model and receiver model in the UV communications.

We further extended the study into the case when ISI effect becomes dominant. Provided with the measurements on channel path loss and impulse response, the perfor-

mance of an NLOS LED-based UV receiver was evaluated semi-analytically in the delay spread channel and we numerically illustrated the typical achievable data rates under different BER requirements in varied transmit/receive geometries. This work may be further developed to a pure analytical form when closed forms of path loss and impulse response models are available.

The future work on the NLOS UV communications through the scattering channel can be well developed both theoretically and experimentally. Namely, the introduction of more parameters like beam angle and field of view into the channel models will offer additional degrees of freedom in the analysis. Pulse broadening after a NLOS propagation channel may be compensated by techniques of advanced transceivers such as the equalization. The link level study is closely related to Poisson communication theory using an IM/DD abstraction and consequently ultimate performance limits in terms of Shannon capacity shall be unveiled. Overall, the NLOS UV communications offers a fertile soil for researchers.

Chapter 4

Opportunistic User Cooperation for Turbulent FSO Link

It is introduced in Chapter 1 that the free space optical (FSO) communications over medium to long range is challenged by the turbulence induced fading. In contrast to the NLOS UV communications utilizing the LED array, FSO link has to take advantage of a high power laser and narrow beam to reach further distance in a line-of-sight path. In this chapter, we will propose techniques to minimize the fading effect for FSO communications. Especially, we consider the user cooperation to clear the obstacle, which is regarded as a special form of MIMO techniques. Both the decode and forward (DF) and amplify and forward (AF) relays will be adopted and discussed in Section 4.3 in an information theoretic perspective. Simulation and numerical analysis are to be presented in Section 4.4.

4.1 Introduction

Different from the NLOS UV communications, an IR based free space optical (FSO) communication link features a line-of-sight transmission path, abundant unlicensed bandwidth and rapid deployment. As an optical solution, it is favored to provide high throughput data access. Similar to the NLOS UV communication link, most FSO communication systems also employ the scheme of intensity modulation and direct detection (IM/DD) to relieve the complexity requirement associated with coherent schemes. In contrast to NLOS scattering channel, a FSO link is overshadowed by many detrimental effects of atmospheric channel such as attenuation and turbulence which render a weak signal intensity and random fluctuations called turbulence induced fading.

To cope with the attenuation effect due to channel absorption, a communication system design needs to plan the link budget carefully while the turbulence effect is caused by the inhomogeneities in the temperature and pressure of atmosphere. As a consequence the fading impairs the received signal, which must be properly mitigated [6], [38], [41]. From the theory of wireless communications, we know various techniques can be utilized to combat against fading such the frequency, time and spatial diversity schemes. When it comes to the FSO system, both time and spatial techniques are extensively studied and applied. For example, the time domain approaches involve the error-control codes (ECC) at the transmitter side [13], [64],[76] or the maximum likelihood sequence detection (MLSD) [14], [75] at the receiver. However in reality, turbulence induced channel fade may last as long as tens of milliseconds, and it was soon recognized ECC and MLSD alone can become prohibitively complex and pricey because the anticipated high throughput of FSO link on the order of Gbps demands huge interleaver memory. To obviate the barrier, people start to consider the spatial diversity

technique and universal figures of merits like outage rate [43], uncoded symbol error probability (SEP) [69] and bit error rate (BER) [49] are thoroughly studied in literature. It is also worthwhile to mention, an information theoretic study on the MIMO FSO and fading FSO channel capacity have been proposed in [12], [23], [28] which are based on an ideal Poisson counting model instead of Gaussian noise assumption. In the context, fading FSO channel is assumed to follow a so-called doubly Poisson random process. Channel capacity or bounds on the channel capacity was determined by maximization of the mutual information derived from the statistics.

As an innovative extension, cooperative diversity is a novel approach to leverage the spatial diversity promised by the cooperating relays. In general, studies on a relayed communication channel are largely attributed to the pioneering works by Van der Meulen [65], Cover and El Gamal [19]. There has been a burst of publications on the application of relays to provide the user cooperation during the recent years. Sendonaris *et al* [55],[56], Laneman *et al* [42] have characterized the outage, erogodic capacity, BER performance on various cooperation protocols aided by decode and forward (DF) or amplify and forward (AF) relays. Hunter and Nosratinia [36], [37] extended the manners of cooperation by integrating with rate compatible punctured coding (RCPC). In contrast to the active research activities on cooperative communication in the radio frequency (RF) community, it was not until recently that FSO scholars started to investigate the benefits of relay and relay based user cooperation against fading effect. By noticing the fact that the turbulence can be dependent on the propagation distance, Safari-Uysal formulated a mathematical model on FSO serial and parallel relayed links in [54], where the number of relays can be arbitrary and Gaussian model is the assumption on noise. Targeting on a three-way system scenario, Karimi [39] derived the BER performance of a cooperative FSO link which is enhanced by convolutional code and Abou-Rjeily [2]

obtained semi-analytical results of BER performance assuming ideal photon counting model. To this end, it is clear modeling methodology of FSO study typically involves two flavors. One is the Gaussian channel scenario while the other is built upon Poisson statistics. We comment in the range of infrared (IR) for FSO, the background noise in addition to device noise is substantially much higher than that of UV-C, and the statistics appears closer to Gaussian distributed. Hence we are motivated to adopt AWGN as our major premise.

Confronted with the question on link robustness and inspired by the idea of opportunistic cooperation proposed in the RF wireless communications [27],[77], we intend to reveal the effect of source-relay channel condition on the overall performance of the cooperative FSO link. Of direct relevance to our work are the studies reported in [54], [2] and [77]. To delimit our contribution in a clearer manner, we have following comments.

- Authors proposed in [77] an opportunistic way of cooperation to provide the spatial diversity against Rayleigh fading for RF systems. We thereby envisage a FSO system equipped with a duplex link or at least a simple feedback uplink between the relay and source. Thus partial channel state information (CSI) about the outage shall be available at the source to enable the opportunistic transmission.

- We further employ the formulation of parallel relay model in [54] to consider a three-way configuration composed of a relayed link (source-relay-destination) and a direct transmission (source-destination) link. This is a special case of a parallel relayed FSO system, but there is cooperative signalling involved in the setup.

- In [2], the BER results were derived on the basis of modeling the output of an optical receiver as a Poisson distributed random variable and only DF relay was

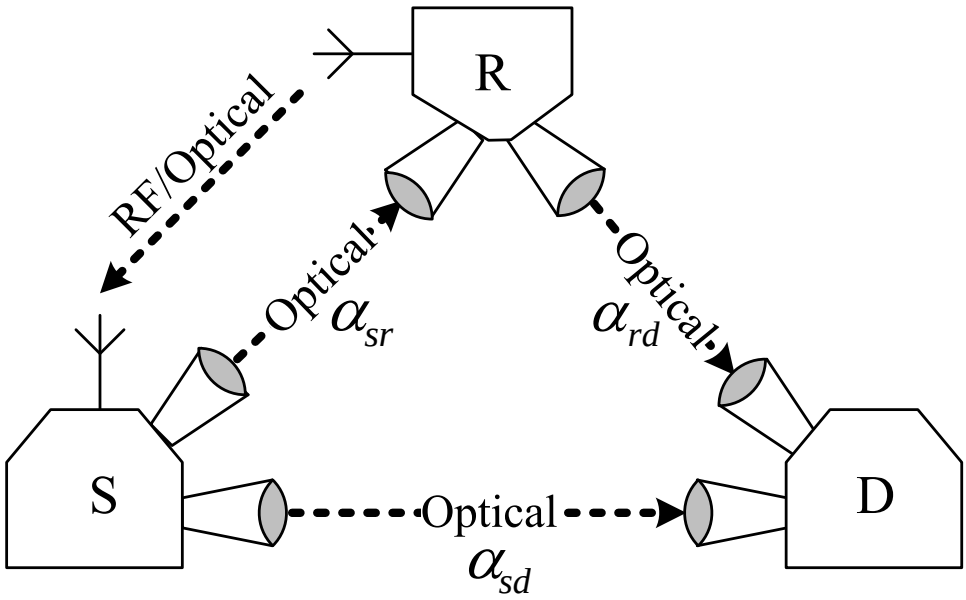

Figure 4.1: A three-way FSO network for opportunistic cooperation.

studied. We instead choose to analyze the outage probability of an opportunistic cooperative FSO system under the effect of turbulence in the presence of thermal noise at the receiver output. Thermal noise is modeled as additive white Gaussian noise (AWGN) in our formulation and both DF and AF relays are considered.

4.2 System Description and Channel Model

This section gives an overview on the system configuration of cooperative FSO. The configuration is the basis of the cooperation protocol between different parties involved in a transmission. Then, we give some information on the characteristics of LOS FSO channel including the path loss model and the turbulence fading model. We will see, in a similar fashion as those for NLOS UV channel, they are central elements to build our framework of analysis.

4.2.1 System Configuration and Protocol

A FSO link aided by a cooperative relay is illustrated in Fig. 4.1. The source (S) transmitter illuminates towards the destination receiver and the relay (R). The transceiver of the relay receives the signal copies from the source and re-transmits to the destination (D) which is essentially a repeating process. Although the setup resembles that of a RF cooperation system, there are some significant differences as claimed by [39],[2] in that a typical FSO system is non-broadcasting and directional in nature because of the narrow beam angle. To resolve this, a FSO source transmitter has to be equipped with dual Tx apertures pointing to the relay and the destination respectively while the destination receiver needs two Rx apertures aiming at both the source and the relay. Traditionally, the processing at the relay may assume either DF or AF. A DF relay first decodes the received source signal and regenerates the results of detection. An AF relay works by restoring the analog signal waveform through biasing and scaling before signal regeneration. A significant difference from DF is the distortion induced by the fading effect in the source-relay channel will be accumulated and conveyed to the destination in AF link. The design of AF relay usually requires the operation in analog domain such as the scaling function which may be implemented using automatic gain control (AGC) module while DF relay involves analog to digital and digital to analog conversion. We will give mathematical interpretations on the two relay processing schemes in the next section.

Conceptually, An opportunistic protocol involves a two-step process including a direct transmission (DT) phase and a DF/AF phase.

1. In the first phase (DT), the source transmits towards the relay with power P_1. The relay picks up the source signal and regenerates it in the second step if there

is no outage occurred to the S-R link.

2. In the second phase (DF/AF), if source-relay outage happens to DT phase, the source should use the S-D link with all of the remaining power (P_2+P_3); otherwise, the relay and the source simultaneously re-transmit to the destination with powers P_2 and P_3 respectively. We comment because the transmitter at the source has two apertures pointing to the relay and the destination respectively, the source can always individually selects which link to be activated for transmission depending on the S-R link condition.

To aid the opportunistic mechanism, we assume that a feedback R-S link is enabled by a hybrid FSO relay transceiver mounted with a low cost RF antenna or other optical source in a different wavelength, which offers the duplex capability. Furthermore, through proper frame design, in-band signalling indicates to the destination which link contributes the received signal copy. By comparison, for a deterministic cooperation as proposed in [2], the relay always cooperates with the source by regenerating with power P_2 in the DF/AF phase while the source communicates with the destination using power P_3 simultaneously. Note that the constraint on the total power consumption P_{tot} maintains $P_1+P_2+P_3 = P_{tot}$ for a fair comparison with the direct transmission which is non-cooperative. A simple power allocation for cooperative system is an equal division of the total power such that $P_1 = P_2 = P_3 = P_{tot}/3$.

4.2.2 Channel Model on Attenuation and Turbulence

In Fig. 4.1, the propagation of light signal experiences the atmospheric attenuation and turbulence effect along each pairs of terminals. The channel model can be

referred in [54]

$$g = \alpha^2 L(d) \tag{4.1}$$

where $L(d)$ is the distance dependent path loss without normalization as a minor difference from [54]. According to the path loss equation in [11], the amount of received optical power is a function of the beam divergence Ω, the receiver aperture area A_r, the link range d as well as the atmospheric attenuation coefficient ξ

$$L(d) = \frac{A_r}{(\Omega \cdot d)^2} exp(-\xi \cdot d). \tag{4.2}$$

It is clear as in eqn. (4.2), the path loss is closely to the distance and can be reduced if the receiver has a big enough receiver aperture size to collect the energy.

For another, numerous literature has been devoted to the modeling of channel fading amplitude $\alpha = \exp(\chi)$ due to atmosphere turbulence, where χ is the log-amplitude. As indicated by chapter 1, it is a common agreement that log-normal probability distribution can be applicable in the case of weak turbulence and the Gamma-Gamma distribution good for the case of medium or strong turbulence [63]. For the log-normal distribution, we have

$$f(\alpha) = \frac{1}{\sqrt{2\pi\sigma_\chi^2}\alpha} \exp\Big(- \frac{ln(\alpha) - \mu_\chi}{2\sigma_\chi^2}\Big), \tag{4.3}$$

where $\mu_\chi = -\sigma_\chi^2$ to ensure the average power is not further scaled except under the path loss $L(d)$ of FSO channel. The log-amplitude variance σ_χ^2 reflects the strength of fading effect and depends on the distance d, wave number k and the refractive index structure number C_n^2 as

$$\sigma_\chi^2(d) = 0.124 k^{\frac{7}{6}} C_n^2 d^{\frac{11}{6}}. \tag{4.4}$$

As depicted in Fig. 4.1, the links between S-D, S-R and R-D have channel fades denoted as α_{sd}, α_{sr} and α_{rd}. Corresponding path loss ratios are L_{sd}, L_{sr} and L_{rd}.

4.3 Outage Analysis of Cooperative FSO System

Several cooperation strategies are discussed in this section covering non-cooperative transmission (NC), deterministic DF/AF cooperation (dDF/dAF), our proposed opportunistic DF/AF cooperation(oDF/oAF). For the choice on the intensity modulation schemes, being robust against background radiation in terms of maximum likelihood detection, the binary pulse position modulation (BPPM) is adopted. Signal model, SNR representation and outage probability are developed in next subsections.

4.3.1 Non-cooperative Scheme

A direct transmission is initiated from the source to the destination without the aid of relay in the non-cooperative scheme where all of the power $P_{tot} = P$ is allocated to the source transmitter. The BPPM symbol at the destination has different forms of representations in signal slot and non-signal slot

$$r_{NC} = \begin{pmatrix} r^s_{NC} \\ \\ r^n_{NC} \end{pmatrix} = \begin{pmatrix} (P_s g_{sd} + RT_s P_b) + n^s_d \\ \\ RT_s P_b + n^n_d \end{pmatrix}, \tag{4.5}$$

where the channel gain $g_{sd} = \alpha^2_{sd} L(d_{sd})$ and we define $P_s = RPT_s$ as the effective transmitted power during a transmission period T_s. The receiver is subject to background radiation with power P_b. Electronic domain thermal noise n^s_d, n^n_d can be modeled as AWGN which has a probability density function of $N(0, \frac{\sigma^2_n}{2})$. σ^2_n depends on the load resistor of the transimpediance amplifier circuit through the function $\sigma^2_n = (2\kappa_b T^o / R_L) T_s$ where κ_b is the Boltzmann constant and T^o is the absolute temperature. $R = \eta q / hf$ is defined as the responsitivity of the photodetector with which optical receiver converts the optical power into electrical signal. η is the quantum efficiency; q is the electron's charge; h is the planck constant and f is the operating frequency of laser.

In [54], definitions of electronic SNR and outage probability have been presented which may be referred in [22] and [10] as well. We cite them as below

$$\Gamma = \frac{(\mu^s - \mu^n)^2}{\sigma_n^2}. \tag{4.6}$$

μ^s and μ^n are the average powers during signal and non-signal slots. For a communication system, reliable transmission rate R_0 is linked to SNR Γ through Shannon formula and an outage event is defined when instantaneous transmission rate $R = \log(1+\Gamma)$ is less than R_0. Due to the randomness of FSO channel, outage probability is introduced to characterize the link robustness besides BER

$$P_{out}(R_0) = Pr\{\log_2(1+\Gamma) < R_0\} = Pr\{\Gamma < \Gamma_{th}\}. \tag{4.7}$$

where $\Gamma_{th} = 2^{R_0} - 1$.

From eqns. (4.5) and (4.6), the SNR of a non-cooperative S-D link is

$$\Gamma_{NC} = \frac{(g_{sd}P_s)^2}{\sigma_n^2}. \tag{4.8}$$

And the corresponding outage probability is expressed as

$$\begin{aligned} P_{out,NC} &= Pr\{\Gamma_{NC} < \Gamma_{th}\} \\ &= Pr\left\{\alpha_{sd}^2 < \sqrt{\frac{\Gamma_{th}\sigma_n^2}{(L_{sd}P_s)^2}}\right\} \\ &= Q\left(\frac{ln(K_{sd,th,NC}) - 2\sigma_\chi^2(d_{sd})}{2\sigma_\chi(d_{sd})}\right). \end{aligned} \tag{4.9}$$

The second equality in eqn. (4.9) is obtained by plugging in eqn. (4.8) and $K_{sd,th,NC}$ is a constant denoting $\sqrt{\frac{(L_{sd}P_s)^2}{\Gamma_{th}\sigma_n^2}}$. Eqn. (4.9) can be easily solved using Q function since α_{sd}^2 is also a log-normal random variable with $LN(-2\sigma_\chi^2, 4\sigma_\chi^2)$. The Q function is defined as $Q(x) = \int_x^\infty \frac{1}{\sqrt{2\pi}} exp\big(-\frac{\alpha^2}{2}\big) d\alpha$.

4.3.2 Deterministic Cooperation

Deterministic cooperation can be viewed as a special case of the parallel FSO relay proposed in [54]. The cooperation involves the participation of a relayed link from source to destination via relay and a direct transmission link from source to destination, both of which form a parallel link. As aforementioned, the cooperation protocol requires a direct transmission over S-R link during the DT phase while the retransmissions through the R-D/S-D links are activated during the DF/AF phase. Depending on the processing at the relay, the derivation of SNR and outage probability model can be distinct. We will address them separately in the next sub-sections.

4.3.2.1 Deterministic cooperation aided by DF relay

Notice the parallel links in nature, dDF is a cooperation scheme where user data and its copy are received by the destination from the source and relay respectively in the DT and DF time phases. An outage happens to parallel links only if neither of them could succeed and the overall outage probability can be defined in eqn. (4.10) as follows

$$P_{out,dDF} = P_{out,sd} \cdot P_{out,srd,DF}. \tag{4.10}$$

Since $P_{out,sd}$ is the outage probability for the direct transmission link from source to destination during the first time period, it follows the same form as that of the non-cooperation case except the power consumption is $\frac{P}{3}$. Regarding the link of S-R-D, in essence it is a one hop serial decode and forward relayed link and we have,

$$P_{out,srd,DF} = 1 - (1 - P_{out,sr})(1 - P_{out,rd}). \tag{4.11}$$

$P_{out,sr}$ and $P_{out,rd}$ are outage probabilities for each segment of the DF relayed link which can be also written in the form of Q function with different channel gains.

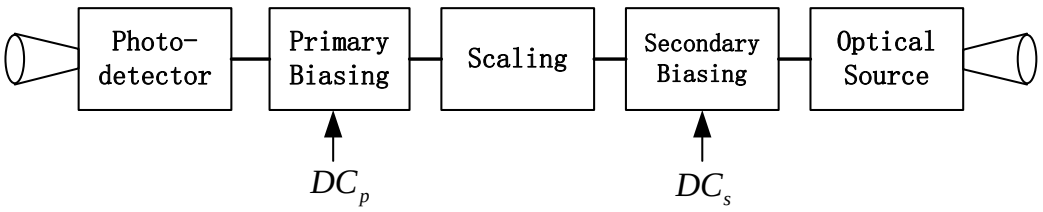

Figure 4.2: AF relay processing.

To summarize, eqn. (4.10) is expressed as

$$P_{out,dDF} = Q\left(\frac{ln(K_{sd,th,dDF}) - 2\sigma_\chi^2(d_{sd})}{2\sigma_\chi(d_{sd})}\right) \times \left\{1 - \left[1 - Q\left(\frac{ln(K_{sr,th,dDF}) - 2\sigma_\chi^2(d_{sr})}{2\sigma_\chi(d_{sr})}\right)\right] \times \left[1 - Q\left(\frac{ln(K_{rd,th,dDF}) - 2\sigma_\chi^2(d_{rd})}{2\sigma_\chi(d_{rd})}\right)\right]\right\}. \quad (4.12)$$

where

$$K_{sd,th,dDF} = \sqrt{\frac{(L_{sd}P_s/3)^2}{\Gamma_{th}\sigma_n^2}}$$
$$K_{sr,th,dDF} = \sqrt{\frac{(L_{sr}P_s/3)^2}{\Gamma_{th}\sigma_n^2}}$$
$$K_{rd,th,dDF} = \sqrt{\frac{(L_{rd}P_s/3)^2}{\Gamma_{th}\sigma_n^2}}.$$

4.3.2.2 Deterministic cooperation aided by AF relay

When it comes to an AF relay as depicted by Fig. 4.2, the source signal is picked up, biased, scaled, re-biased and re-transmitted. The biasing DC_p is added to remove the DC portion due to the background radiation P_b while the scaling operation is applied to extract the channel fading coefficient of S-R link from the signal slot.

However, constrained by the nonnegativity requirement on the optical signal, we intentionally introduce a secondary DC biasing DC_s to raise the electrical signals above zero. The selection of DC_s can be operated manually. With manual adjustment,

DC_s is a constant set point which has to be appropriately determined. When DC_s takes such a low level that the output after secondary biasing becomes negative for either slot of a BPPM symbol, the analog relay transceiver could shut off the retransmission whenever it detects the occurrence through the circuit level comparator. In this event, the destination receiver sees no effective contribution from the relay and the performance loss is expected as a result. In our discussion, it is assumed the secondary biasing can be chosen in a way to avoid such "cutoff" event and it can be shown the actual value of DC_s does not affect the analysis and the results.

To obtain the signal representation, first over the S-R link, the received signal is

$$r_{sr} = \begin{pmatrix} r_{sr}^s \\ r_{sr}^n \end{pmatrix} = \begin{pmatrix} (\frac{P_s}{3} g_{sr} + P_b) + n_r^s \\ RT_s P_b + n_r^n \end{pmatrix}. \tag{4.13}$$

At the relay, we choose the DC bias to be $DC_p = -RT_s P_b$. After biasing,

$$\begin{aligned} r_{sr,biased} &= \begin{pmatrix} (\frac{P_s}{3} g_{sr} + P_b) + n_r^s + DC_p \\ RT_s P_b + n_r^n + DC_p \end{pmatrix} \\ &= \begin{pmatrix} \frac{P_s}{3} g_{sr} + n_r^s \\ n_r^n \end{pmatrix}. \end{aligned} \tag{4.14}$$

The scaling operation is applied to the biased signal by a factor of $a_r = 1/E[r_{sr,biased}^s + r_{sr,biased}^n] = \frac{3}{P_s L_{sr}}$, which yields

$$r_{sr,biased,scaled} = \begin{pmatrix} \alpha_{sr}^2 + a_r n_r^s \\ a_r n_r^n \end{pmatrix}. \tag{4.15}$$

Before the retransmission, a secondary biasing is added to ensure the non-negativity of electrical domain signal reconstructions such that

$$r_{sr,biased,scaled}^+ = \begin{pmatrix} \alpha_{sr}^2 + a_r n_r^s + DC_s \\ a_r n_r^n + DC_s \end{pmatrix}. \tag{4.16}$$

The signal can then be retransmitted with power $\frac{P}{3}$ over R-D link. The destination receiver detects the signal from AF relay as below

$$r_{srd} = \begin{pmatrix} \left[\frac{P_s}{3} g_{rd}(\alpha_{sr}^2 + a_r n_r^s + DC_s) + P_b\right] + n_{srd}^s \\ \left[\frac{P_s}{3} g_{rd}(a_r n_r^n + DC_s) + P_b\right] + n_{srd}^n \end{pmatrix}. \tag{4.17}$$

We consider an equal gain combining (EGC) receiver at the destination which produces the electronic signal by taking into account both copies from the source r_{sd} and the AF relay r_{srd}

$$\begin{aligned} r_{dAF} =& r_{sd} + r_{srd} \\ =& \begin{pmatrix} (\frac{P_s}{3} g_{sd} + P_b) + n_d^s \\ RT_s P_b + n_d^n \end{pmatrix} + \\ & \begin{pmatrix} \left[\frac{P_s}{3} g_{rd}(\alpha_{sr}^2 + a_r n_r^s + DC_s) + RT_s P_b\right] + n_{srd}^s \\ \left[\frac{P_s}{3} g_{rd}(a_r n_r^n + DC_s) + RT_s P_b\right] + n_{srd}^n \end{pmatrix}. \end{aligned} \tag{4.18}$$

According to eqn. (4.6), the SNR of dAF cooperation can be obtained by employing the signal representation in eqn. (4.18) and assuming the noise terms n_d and n_{srd} are independent and identically distributed,

$$\Gamma_{dAF} = \frac{\left(g_{sd} + g_{rd}\alpha_{sr}^2\right)^2 (\frac{P_s}{3})^2}{\sigma_n^2 \left(2 + \frac{g_{rd}^2}{L_{sr}^2}\right)}. \tag{4.19}$$

Study on the outage probability of dAF cooperation requires the knowledge on cumulative distribution function (CDF) of Γ_{dAF} which is a function of three random variables α_{sd}^2, α_{rd}^2 and α_{sr}^2. Since the analysis appears non-trivial, we choose to ignore the noise contribution at relay, which yields a upper bound on SNR of dAF cooperation

$$\Gamma_{dAF}^{UB} = \frac{\left(g_{sd} + g_{rd}\alpha_{sr}^2\right)^2 (\frac{P_s}{3})^2}{2\sigma_n^2}. \tag{4.20}$$

We can obtain a lower bound to the outage probability based upon Γ_{dAF}^{UB} by plugging

eqn. (4.20) into eqn. (4.7).

$$\begin{aligned} P_{out,dAF}^{LB} &= Pr\{\Gamma_{dAF}^{UB} < \Gamma_{th}\} \\ &= Pr\left\{\beta < \sqrt{\frac{2\Gamma_{th}\sigma_n^2}{(\frac{P_s}{3})^2}}\right\} \\ &= Q\left(\frac{ln(K_{th,dAF}) + \mu_\beta}{\sigma_\beta}\right), \end{aligned} \tag{4.21}$$

where $K_{th,dAF} = \sqrt{\frac{(\frac{P_s}{3})^2}{2\Gamma_{th}\sigma_n^2}}$ and a new random variable is introduced as $\beta = L_{sd}\alpha_{sd}^2 + L_{rd}\alpha_{rd}^2\alpha_{sr}^2$. To derive the statistics of β, we first define $\alpha_0 = \alpha_{rd}^2\alpha_{sr}^2$ which is still a log-normal random variable with the distribution $LN(\mu_{\alpha_0}, \sigma_{\alpha_0}^2) = LN\big(-2[\mu_\chi(d_{sr}) + \mu_\chi(d_{rd})], 4[\sigma_\chi^2(d_{sr}) + \sigma_\chi^2(d_{rd})]\big)$. Now that the random variable β is a weighted sum of two log-normal random variables α_{sd}^2 and α_0. It is introduced in [54] that β can be approximated by another log-normal random variable using moment matching method

$$\mu_\beta = \ln\big(L(d_{sd}) + L(d_{rd})\big) - \sigma_\beta^2, \tag{4.22}$$

$$\sigma_\beta^2 = \ln\left[1 + \left(\frac{L_{sd}\big(e^{4\sigma_\chi^2(d_{sd})} - 1\big)}{(L_{sd} + L_{rd})^2} + \frac{L_{rd}\big(e^{4\sigma_{\alpha_0}^2} - 1\big)}{(L_{sd} + L_{rd})^2}\right)\right]. \tag{4.23}$$

4.3.3 Opportunistic cooperation

In this section, we propose the idea of opportunistic cooperation utilizing DF or AF relay to be applied to the FSO links in an attempt to enhance the system.

4.3.3.1 Opportunistic cooperation aided by DF relay

The opportunistic cooperation involves the participation of the DF relay depending on the S-R link quality. In case of S-R outage, the relay notifies the source to repeat the transmission of the signal with all the remaining power over the feedback link; otherwise, the relay will decode and forward the copy. When S-R link meets the

SNR requirement, the EGC receiver output is contributed by both the source and the cooperative DF relay with the combined signal r_{oDF-DF} in the following form

$$\begin{aligned} r_{oDF-DF} = r_{sd} + r_{rd} &= \begin{pmatrix} r_{sd}^{s} \\ \\ r_{sd}^{n} \end{pmatrix} + \begin{pmatrix} r_{rd}^{s} \\ \\ r_{rd}^{n} \end{pmatrix} \\ &= \begin{pmatrix} (\frac{P_s}{3} g_{sd} + RT_s P_b) + n_d^s \\ \\ RT_s P_b + n_d^n \end{pmatrix} + \\ &\quad \begin{pmatrix} (\frac{P_s}{3} g_{rd} + RT_s P_b) + n_{rd}^s \\ \\ RT_s P_b + n_{rd}^n \end{pmatrix} \\ &= \begin{pmatrix} [\frac{P_s}{3}(g_{sd} + g_{rd}) + 2RT_s P_b] + N_d^s \\ \\ 2RT_s P_b + N_d^n \end{pmatrix}. \end{aligned} \tag{4.24}$$

Note that $N_d = n_d + n_{rd}$. n_d and n_{rd} are independent and independently distributed in our analysis. To evaluate the outage, we first obtain the SNR as

$$\Gamma_{oDF-DF} = \frac{(g_{sd} + g_{rd})^2 (\frac{P_s}{3})^2}{2\sigma_n^2}. \tag{4.25}$$

Let $\theta = g_{sd} + g_{rd}$, then the outage probability in this case is

$$\begin{aligned} P_{out,oDF-DF} &= Pr\left\{ \theta < \sqrt{\frac{2\Gamma_{th}\sigma_n^2}{(\frac{P_s}{3})^2}} \right\} \\ &= Q\left(\frac{ln(K_{th,oDF-DF}) + \mu_\theta}{\sigma_\theta} \right), \end{aligned} \tag{4.26}$$

where $K_{th,oDF-DF} = \sqrt{\frac{(\frac{P_s}{3})^2}{2\Gamma_{th}\sigma_n^2}}$ and θ is a weighted sum of two log-normal random variables $(\alpha_{sd}^2, \alpha_{rd}^2)$. Again by using moment matching method, we have

$$\mu_\theta = \ln\big(L(d_{sd}) + L(d_{rd})\big) - \sigma_\theta^2, \tag{4.27}$$

$$\begin{aligned} \sigma_\theta^2 = \ln\Bigg[1 + \Bigg(&\frac{L_{sd}\big(e^{4\sigma_\chi^2(d_{sd})} - 1\big)}{(L_{sd} + L_{rd})^2} + \\ &\frac{L_{rd}\big(e^{4\sigma_\chi^2(d_{rd})} - 1\big)}{(L_{sd} + L_{rd})^2} \Bigg) \Bigg]. \end{aligned} \tag{4.28}$$

Overall outage probability of oDF can be expressed by covering both cases such as the cooperation mode (oDF-DF) and non-cooperative mode (oDF-DT) in which the direct transmission has to be enforced with all the remaining power $\frac{2P}{3}$ in case of S-R link outage

$$\begin{aligned} P_{out,oDF} =& P_{out,sr}P_{out,oDF-DT}+ \\ & (1-P_{out,sr})P_{out,oDF-DF}, \end{aligned} \tag{4.29}$$

where the cooperation mode outage $P_{out,oDF-DF}$ is given in eqn. (4.26); $P_{out,sr}$ can be traced back in the subsection 4.3.2.1 and the direct transmission mode outage $P_{out,oDF-DT}$ is similar to $P_{out,sd}$ except that the former has doubled signal power

$$\begin{aligned} P_{out,oDF-DT} &= Pr\left\{\alpha_{sd}^2 < \sqrt{\frac{\Gamma_{th}\sigma_n^2}{(L_{sd}\frac{2P_s}{3})^2}}\right\} \\ &= Q\left(\frac{ln(K_{sd,th,oDF-DT}) - 2\sigma_\chi^2(d_{sd})}{2\sigma_\chi(d_{sd})}\right), \end{aligned} \tag{4.30}$$

where $K_{sd,th,oDF-DT} = \sqrt{\frac{(L_{sd}\frac{2P_s}{3})^2}{\Gamma_{th}\sigma_n^2}}$.

4.3.3.2 Opportunistic cooperation aided by AF relay

The analysis of outage probability of opportunistic AF follows the footprints of oDF and the overall outage can be elaborated by Bayesian rule as

$$\begin{aligned} P_{out,oAF} =& P_{out,sr}P_{out,oAF-DT}+ \\ & (1-P_{out,sr})P_{out,oAF-AF}. \end{aligned} \tag{4.31}$$

In eqn. (4.31), $P_{out,oAF-DT} = P_{out,oDF-DT}$ as the direct transmission mode is essentially a repetitive coding for both oDF and oAF.

As for the cooperation mode oAF-AF, the destination receiver mode combines the signals from the source and via the relay. Since the signal representation and SNR

analysis have been presented in Section 4.3.2.2, it is straightforward to set $P_{out,oAF-AF}$ equal to $P^{LB}_{out,dAF}$ as in eqn. (4.21) and derive a lower bound to the overall oAF outage probability accordingly

$$P^{LB}_{out,oAF} = P_{out,sr}P_{out,oAF-DT} + (1 - P_{out,sr})P^{LB}_{out,dAF}. \tag{4.32}$$

We leave the exact characterization on oAF outage probability $P_{out,oAF}$ to the numerical study in the next section.

4.4 Numerical Results and Discussion

This section presents numerical results on the analytical forms of outage probabilities related to several cooperation strategies. Monte-carlo simulations are performed to validate the analysis results up to certain order in view of the complexity. Unless otherwise noted, the system parameters in the numerical study are listed in Table 4.1. All the figures given in this section are cited from our works [31] and [32].

Table 4.1: System parameters for numerical analysis

Parameter:	Value:
Wavelength c/f	1550 nm
Atmospheric attenuation coefficient ξ	0.5 dB/km
Temperature T_0	400 K
Refractive index structure C_n^2	5.06×10^{-14} $m^{-2/3}$
Quantum efficiency η	0.75
BPPM slot duration T_s	1 ns
Load resistor R_L	50 Ω
Beam divergence Ω	2 $mrad$
Receiver aperture diameter D	20 cm
Source-destination distance d_{sd}	1000 $meter$

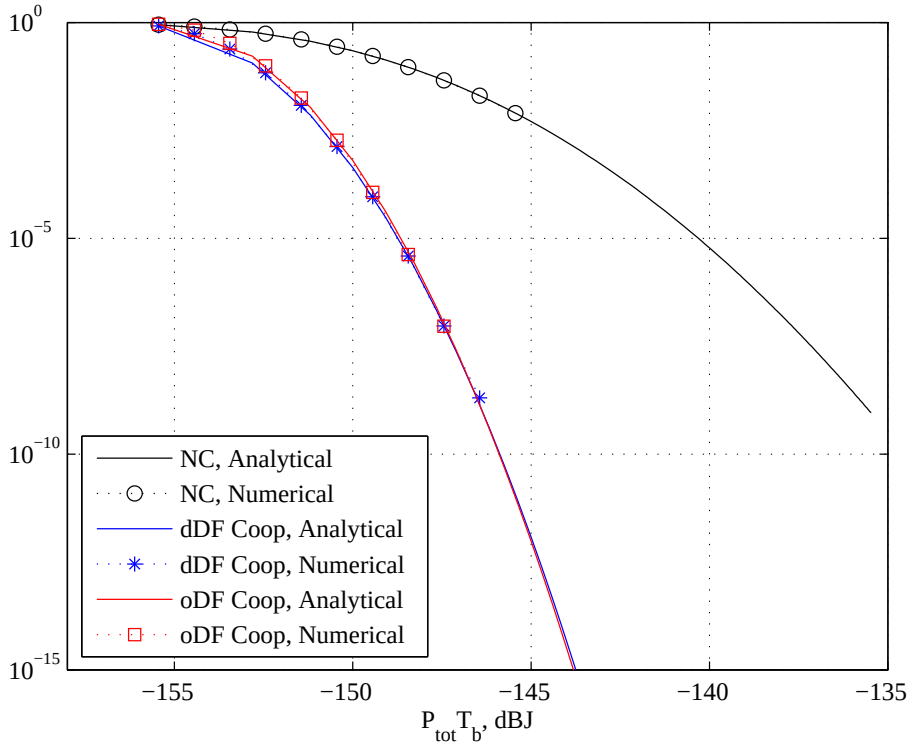

Figure 4.3: Outage performance of opportunistic FSO system aided by DF relay, $d_{sr} = d_{rd} = 500m, d_{sd} = 1000m$.

In Fig. 4.3, we compare the performances of a NC link, a dDF link and an oDF link with both analytical and numerical results plotted. The setup has S-R and R-D distances at 500 meters, which means the relay on the middle spot of the S-D FSO link as a special case. Analytical results are calculated according to eqns. (4.9), (4.12) and (4.29). Monte-Carlo simulations confirm the analytical results. Both dDF and oDF excel NC scheme by around $9dB$ at the outage probability of 10^{-6}. oDF's curve almost overlaps that of dDF, which implies the low outage in S-R segment does not call out the benefit of oDF as expected. By contrast, we present the performance of AF aided cooperative FSO system in Fig. 4.4. Analytical results are calculated by following eqns. (4.9), (4.21) and (4.32). As illustrated, the performance lower bounds of dAF and oAF only give very loose projections on the actual performances backed up by simulations.

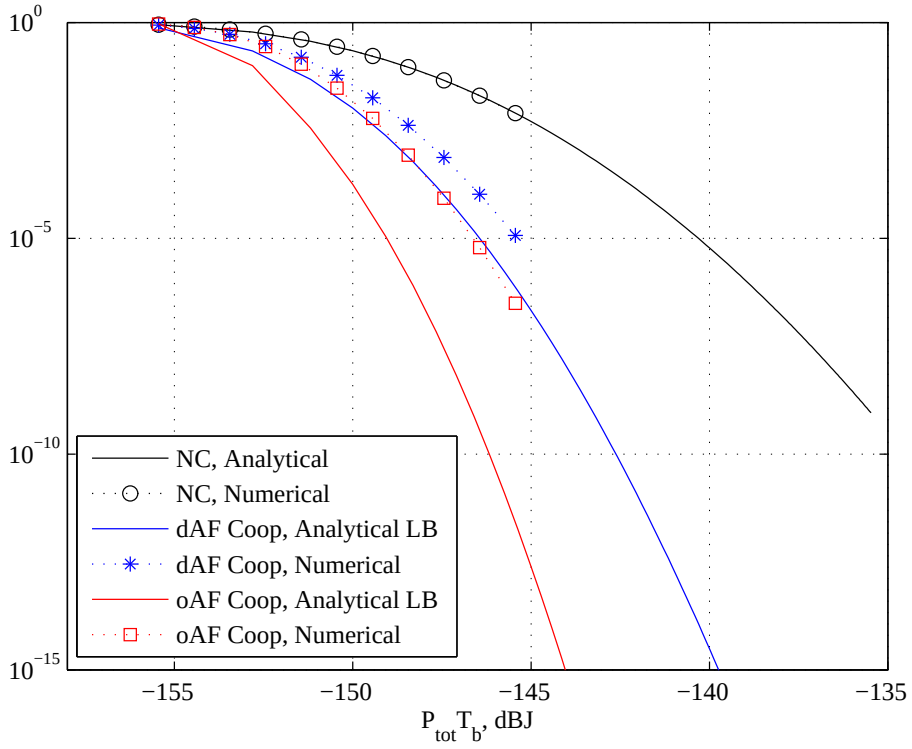

Figure 4.4: Outage performance of opportunistic FSO system aided by AF relay, $d_{sr} = d_{rd} = 500m, d_{sd} = 1000m$.

However, it is clear the AF aided cooperation does improve the link outage by about $7dB$ at 10^{-6} in comparison with that of non-cooperative link. oAF slightly outperforms dAF and the gap increases as the total power consumption ramps up.

In Figs. 4.5 and 4.6, we intend to demonstrate the tradeoff in oDF/oAF as S-R and R-D links become longer. For example, when the link distances of S-R and R-D increase to 1000 meters, both path loss and turbulence effects build up. To illustrate, we evaluate the crossing point at which cooperation scheme is taken over by non-cooperation(NC) operation. It is shown in Fig. 4.5 that oDF is $5dB$ better than dDF. As for AF cooperation FSO system, numerical results indicate neither oAF nor dAF works better than NC in the considered setup of range. We do notice a trend which appears oAF may intersects NC's curve in high power regime. Overall, opportunistic

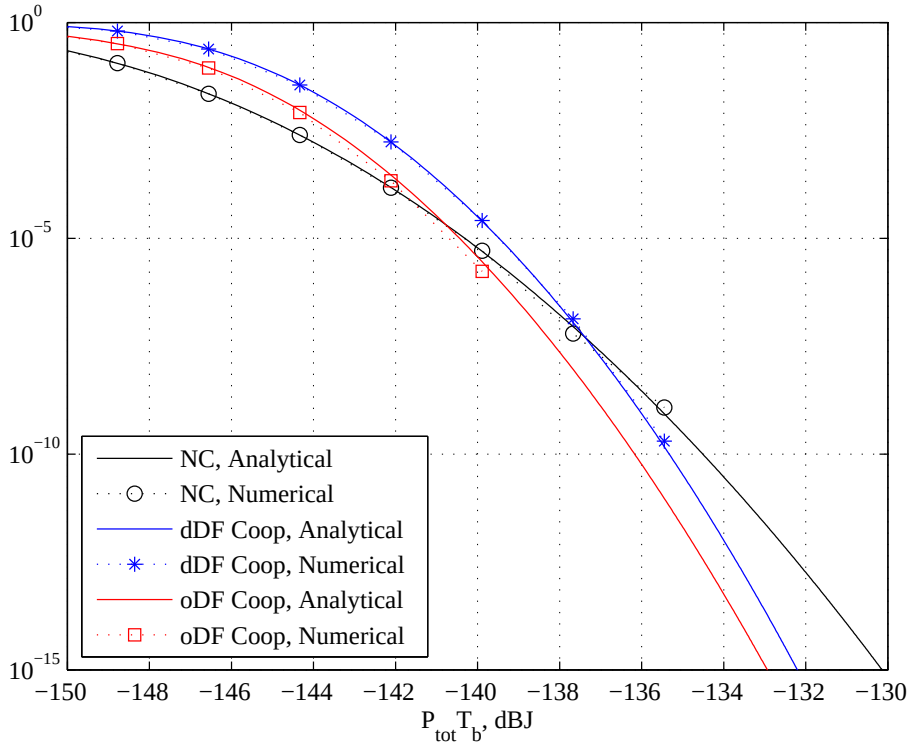

Figure 4.5: Outage performance of opportunistic FSO system aided by DF relay, $d_{sr} = d_{rd} = d_{sd} = 1000m$.

cooperation provides a wider range of tradeoff in terms of sustaining the link at a cost of higher outage rate than deterministic cooperation.

In Fig. 4.7, we study the effect of S-R link quality on performance of cooperation numerically. The S-R separation is varied from 500 to 1000 meters while S-R and R-D distances are set to be 1000 meters. As S-R link distance increases, both oDF and oAF are observed to provide lower outage rate than their deterministic opponents in a consistent way. We also observe when d_{sr} extends beyond 1000 meters, the relayed link starts to play a role via amplify and forward and the oAF outage curve is heading in a decreasing trend. This can be explained by the SNR equation in eqn. (4.19) which has a reduced relay noise contribution $\frac{g_{rd}^2}{L_{sr}^2}\sigma_n^2$ as the ratio of path loss $\frac{L_{rd}}{L_{sr}}$ becomes less than unity. Hence SNR of oAF-AF phase is expected to enhance, resulting in an improved

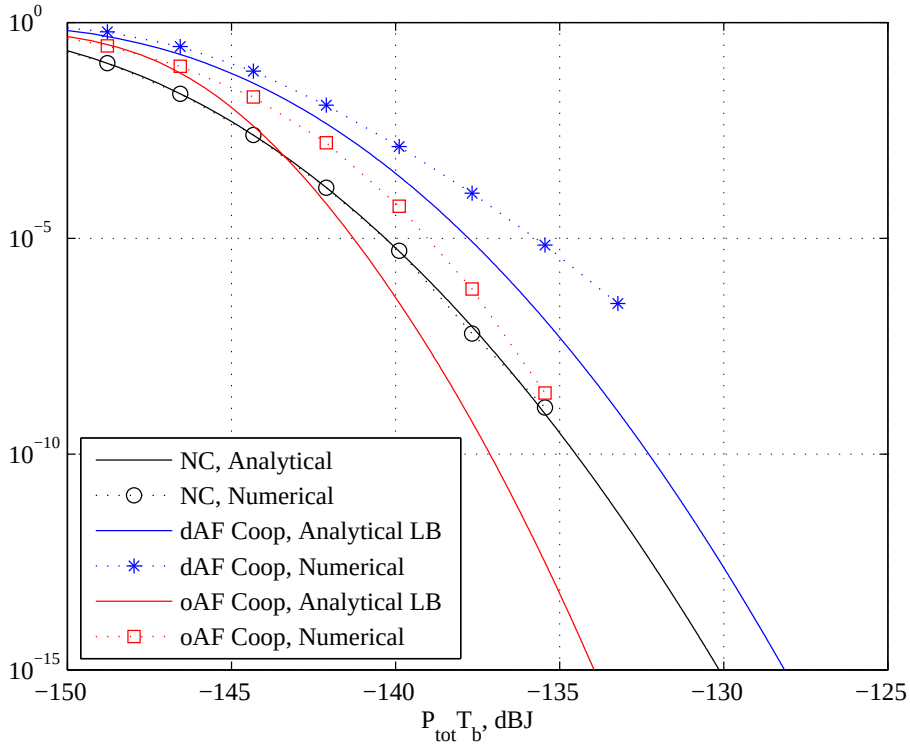

Figure 4.6: Outage performance of opportunistic FSO system aided by AF relay, $d_{sr} = d_{rd} = d_{sd} = 1000m$.

outage.

Fig. 4.8 demonstrates the advantage of opportunistic cooperation over deterministic cooperation as transmission rate varies from 1 to 2.5, which puts higher throughput requirement on the link robustness. Both oDF and oAF outperform deterministic schemes by at least one order lower in terms of the outage rate. For oAF, the difference appears larger in the range of smaller R_0.

4.5 Summary

The opportunistic cooperation concept has been applied to relayed FSO system by extending the schemes of deterministic cooperation. We considered both DF and AF relay. The problem formulation assumes a three-way system configuration and Gaussian

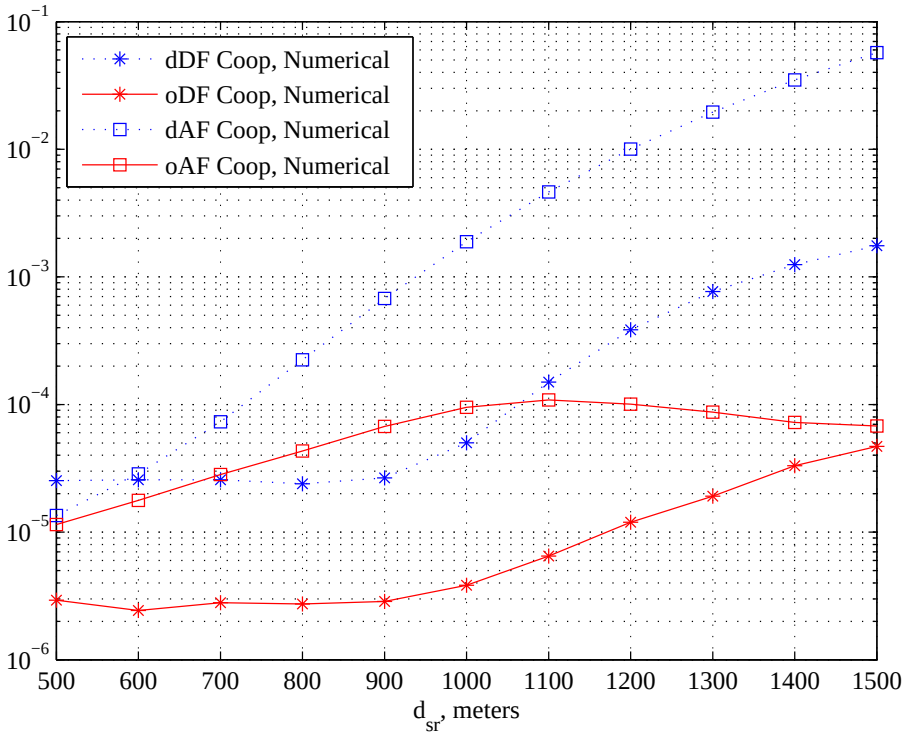

Figure 4.7: Outage performance of opportunistic cooperation vs. S-R link distance, $d_{rd} = d_{sd} = 1000m$.

noise in the electronic domain. Analytical forms of outage probabilities are derived for non-cooperative link, deterministic cooperation and opportunistic cooperation. Monte-Carlo simulations are performed to verify the analytical results.

It is shown oDF achieves the same performance as dDF for close separation of S-R and R-D while oAF excels dAF. When S-R link outage happens more often, oDF/oAF can be adopted to provide a more flexible tradeoff between non-cooperation and user cooperation, which enhances the overall system performance under turbulence induced fading.

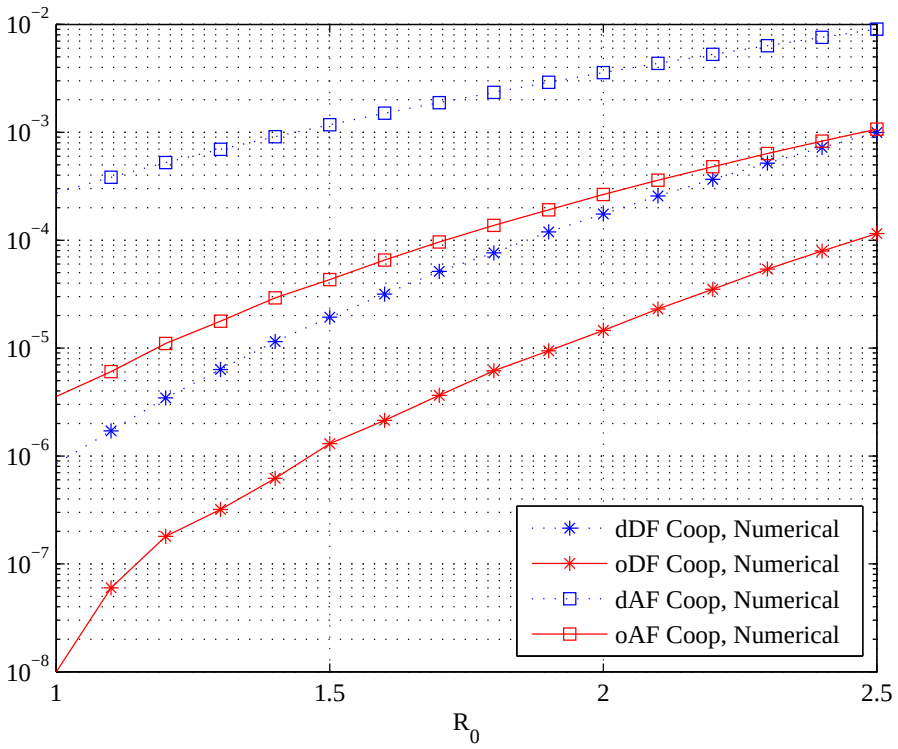

Figure 4.8: Outage performance of opportunistic cooperation vs. transmission rate R_0, $d_{sr} = d_{rd} = d_{sd} = 1000m$.

Chapter 5

Conclusions

In this thesis, we explore the performance limits of outdoor WoC links through the atmospheric channel. Two typical phenomena, namely, the scattering effect and turbulence are investigated by targeting on two ranges of optical wavelengths respectively in UV-C and IR. The uniqueness in UV communications lies in the NLOS propagation path and ultra low background noise, which motivate the applications of a short range, loosely aligned optical link for wireless sensor or ad-hoc network. The IR technology benefits from the huge leap in the advances of device manufacturing and is possible to reach a longer range enabled by a narrow beam light source. Applications in an optical backbone with the rate up to Gbps over a range of 1 km to 10 km are envisioned. As a wireless link, a WoC system is exposed to the challenges arising from several sources. Firstly the scattering results in a huge path loss which limits the achievable range of NLOS UV communication. The multiple paths are also caused by the scatters in the atmosphere such that ISI effect can no longer be ignored for higher rates by introduced interference from neighboring symbols. Another obstacle to the implementation of a WoC link can be the fading effect on the received signal since the wavefront is distorted

and the intensity fluctuates due to turbulence. Lastly device itself may not behave consistently well, the randomness of which has to be properly addressed in the design of an optical receiver. Our research aims to address above issues through theoretical modeling, experimental characterization and numerical analysis.

We characterized the tradeoffs between range and rate for an NLOS UV communication link through the abstraction in a Poisson photon counting model of IM/DD. The analysis incorporates the empirical path loss model of NLOS UV into the error probability derivation, Insights are gained towards how to plan the link budget. Generally speaking, PPM based modulation excels OOK in terms of achievable performance and synchronization. High elevation angles in geometry cause huge path loss such that the signal is attenuated enormously, which demands the adoption of a highly sensitive photodetector to enable communication. To relax the stringent requirements on both a source and a receiver, the concept of NLOS relayed UV link has been proposed. The issue of directional interference is identified and a spatial reuse/time multiplex based MAC layer protocol has been introduced. Numerical results show the potential of such a scheme.

The study on the NLOS UV communications over scattered channel is further extended by considering the implementation of a receiver in which photodector and receiver electronics contribute random gain effect and thermal noise. Our derivation is based upon a ML based detection of OOK and PPM modulations. The output of the photodetector distorted by all sources of noises has been statistically modelled according to the Bayesian rule. Its probability density function is developed and further applied to the detection model. Error performance is successfully obtained in a semi-closed form. Our results reveal the performance difference between PMT and APD based receivers. They help to evaluate the choice on gain control of the amplification process. Within

the framework of a photon counting receiver utilizing PMT, we quantify the influence of scattering induced pulse broadening on the receiver. The NLOS UV link is concluded to be power limited under high elevation angles and bandwidth limited under low elevation angles.

For mid to long range applications in the wavelength of IR, major emphasis is placed on how to minimize the fades that the LOS IR link experiences. We formulate a signal model for a three way of FSO relay links assuming the piecewise link corrupted by log-normal distributed channel fade and Gaussian distributed thermal noise while existing analysis was carried out with Poisson models. In the setup, a FSO relay provides additional diversity to combat fading. We introduce a feeback link between the relay and the source so that the channel state information (CSI) is available at the transmitter to opportunistically exploit the relay link. Numerical results show the outage probability is lowered compared with non-cooperative link, and the performance difference increases for opportunistic cooperation especially when the link condition between source and relay deteriorates for both DF and AF based relays.

Appendix A

Acronyms

AF	Amplify and Forward
AGC	Automatic Gain Control
APD	Avalanche Photodiode
AWGN	Additive White Gaussian Noise
BER	Bit Error Probability
COTS	Commercial Off-The-Shelf
DC	Direct Current
DF	Decode and Forward
DT	Direct Transmission
FoV	Field of View
FSO	Free Space Optics
IM/DD	Intensity Modulation and Direct Detection
IR	Infrared
ISI	Inter-Symbol Interference
LDPC	Low Density Parity Check
LED	Light Emission Diode
LOS	Line-of-Sight
LTI	Linear Time Invariant
MAC	Medium Access Control
MGF	Moment Generating Function
MIMO	Multiple-Input-Multiple-Output
ML	Maximum Likelihood
MLSD	Maximum Likelihood Sequence Detection
NC	Non-Cooperation
NLOS	Non-Line-of-Sight
oAF	Opportunistic AF
oDF	Opportunistic DF
OOK	On-Off Keying
PAT	Pointing, Acquisition and Tracking
PE	Photoelectrons
pdf	Probability Density Function

PMT	Photomultiplier Tube
PPM	Pulse Position Modulation
QE	Quantum Efficiency
RCPC	Rate Compatible Punctured Coding
RF	Radio Frequency
SSL	Solid State Laser
SNR	Signal-to-Noise Ratio
UV	Ultraviolet
WoC	Wireless Optical Communications

Bibliography

[1] C. Abou-Rjeily and S. Haddad. Cooperative fso systems: Performance analysis and optimal power allocation. *Journal of Lightwave Technology*, 29(7):1058 –1065, april1, 2011.

[2] C. Abou-Rjeily and A. Slim. Cooperative diversity for free-space optical communications: Transceiver design and performance analysis. *IEEE Transactions on Communications*, 59(3):658 –663, march 2011.

[3] V. Adivarahan, Q. Fareed, S. Srivastava, T. Katona, M. Gaevski, and A. Khan. Robust 285 nm deep uv light emitting diodes over metal organic hydride vapor phase epitaxially grown aln/sapphire templates. *Japanese Journal of Applied Physics*, 46:537–539, 2007.

[4] J. Akella, M. Yuksel, and S. Kalyanaraman. Error analysis of multi-hop free-space optical communication. In *IEEE International Conference on Communications, 2005. ICC 2005.*, volume 3, pages 1777 – 1781 Vol. 3, may 2005.

[5] S. B. Alexander. *Optical Communication Receiver Design.* SPIE Press, 1997.

[6] L. C. Andrews and R. L. Phillips. *Laser Beam Propagation Through Random Media.* SPIE Optical Engineering Press, 1998.

[7] J. Anguita, I. Djordjevic, M. Neifeld, and B. Vasic. Shannon capacities and error-correction codes for optical atmospheric turbulent channels. *J. Opt. Netw.*, 4(9):586–601, 2005.

[8] X. Bai, D. Mcintosh, H. Liu, and J. C. Campbell. Ultraviolet single photon detection with geiger-mode 4h-sic avalanche photodiodes. *IEEE Photonics Technol. Lett.*, 19:1822–1824, 2007.

[9] M. F. Barsoum, B. Moision, M. P. Fitz, D. Divsalar, and J. Hamkins. Exit function aided design of iteratively decodable codes for the poisson ppm channel. *IEEE Transactions on Communications*, 58(12):3573 –3582, december 2010.

[10] E. Biglieri, J. Proakis, and S. Shamai. Fading channels: information-theoretic and communications aspects. *IEEE Transactions on Information Theory*, 44(6):2619 –2692, oct 1998.

[11] S. Bloom and W. S. Hartley. The last-mile solution: Hybrid fso radio. *White Paper, Airfiber Inc.*, may 2002.

[12] K. Chakraborty, S. Dey, and M. Franceschetti. Outage capacity of mimo poisson fading channels. *IEEE Transactions on Information Theory*, 54(11):4887 –4907, nov. 2008.

[13] V. Chan. Coding for the turbulent atmospheric optical channel. *IEEE Transactions on Communications*, 30(1):269 – 275, jan 1982.

[14] N. D. Chatzidiamantis, M. Uysal, T. A. Tsiftsis, and G. K. Karagiannidis. Iterative near maximum-likelihood sequence detection for mimo optical wireless systems. *Journal of Lightwave Technology*, 28(7):1064 –1070, april1, 2010.

[15] G. Chen, F. Abou-Galala, Z. Xu, and B. M. Sadler. Experimental evaluation of led-based solar blind nlos communication links. *Opt. Expr.*, 16(19):15059–15068, 2008.

[16] G. Chen, Z. Xu, H. Ding, and B. M. Sadler. Path loss modeling and performance trade-off study for short-range non-line-of-sight ultraviolet communications. *Opt. Expr.*, 2008.

[17] G. Chen, Z. Xu, and B. M. Sadler. Experimental demonstration of ultraviolet pulse broadening in short-range non-line-of-sight communication channels. *Opt. Expr.*, 18, 2010.

[18] J. Conradi. The distribution of gains in uniformly multiplying avalanche photodiodes: Experimental. *IEEE Transactions on Electron Devices*, 19(6):713 – 718, jun 1972.

[19] T. Cover and A. E. Gamal. Capacity theorems for the relay channel. *IEEE Transactions on Information Theory*, 25(5):572 – 584, sep 1979.

[20] H. Ding, G. Chen, A. K. Majumdar, B. M. Sadler, and Z. Xu. Modeling of non-line-of-sight ultraviolet scattering channels for communication. *IEEE Journal on Selected Areas in Communications*, 27(9):1535 –1544, december 2009.

[21] I. B. Djordjevic. Ldpc-coded optical communication over the atmospheric turbulence channel. In *Conference Record of the Forty-First Asilomar Conference on Signals, Systems and Computers, 2007. ACSSC 2007.*, pages 1903 –1909, nov. 2007.

[22] S. Dolinar, D. Divsalar, J. Hamkins, and F. Pollara. Capacity of ppm on gaussian and webb channels. In *IEEE International Symposium on Information Theory, 2000. Proceedings.*, page 410, 2000.

[23] A. A. Farid and S. Hranilovic. Diversity gains for mimo wireless optical intensity channels with atmospheric fading and misalignment. In *IEEE Globecom Workshops (GC Wkshps), 2010*, pages 1015 –1019, dec. 2010.

[24] R. M. Gagliardi and S. Karp. *Optical Communications 2nd Ed.* John Wiley and Sons, Inc, New York, 1995.

[25] C. N. Georghiades. Modulation and coding for throughput-efficient optical systems. *IEEE Transactions on Information Theory*, 40(5):1313–1326, Sept. 1994.

[26] J. W. Goodman. *Statistical Optics*. Wiley, New York, 1985.

[27] D. Gunduz and E. Erkip. Opportunistic cooperation by dynamic resource allocation. *IEEE Transactions on Wireless Communications*, 6(4):1446 –1454, april 2007.

[28] S. M. Haas and J. H. Shapiro. Capacity of wireless optical communications. *IEEE Journal on Selected Areas in Communications*, 21(8):1346 – 1357, oct. 2003.

[29] Q He, B. M. Sadler, and Z Xu. Modulation and coding tradeoffs for non-line-of-sight ultraviolet communications. *Proc. SPIE*, 2009.

[30] Q He, B. M. Sadler, and Z Xu. On the achievable performance of non-line-of-sight ultraviolet communications. *Proc. OSA*, 2010.

[31] Q. He and Z. Xu. Opportunistic cooperation for fso links aided by decode and forward relay. In *Accepted by IEEE Globecom Workshops (GC Wkshps), 2012*, pages 1015 –1019, Dec. 2012.

[32] Q. He and Z. Xu. Outage analysis of opportunistic cooperation for fso communication links. *Submitted to Journal of Lightwave Technology*, 2012.

[33] Q. He, Z. Xu, and B. M. Sadler. Non-line-of-sight serial relayed link for optical wireless communications. In *IEEE Military Communications Conference, 2010 - IEEE Milcom 2010*, pages 1588 –1593, 31 2010-nov. 3 2010.

[34] Q. He, Z. Xu, and B. M. Sadler. Performance of short-range non-line-of-sight led-based ultraviolet communication receivers. *Opt. Expr.*, 18(12):12226–12238, 2010.

[35] S. Hranilovic. *Wireless Optical Communication Systems*. Springer, New York, 2005.

[36] T. E. Hunter and A. Nosratinia. Diversity through coded cooperation. *IEEE Transactions on Wireless Communications*, 5(2):283 – 289, feb. 2006.

[37] T. E. Hunter, S. Sanayei, and A. Nosratinia. Outage analysis of coded cooperation. *IEEE Transactions on Information Theory*, 52(2):375 – 391, feb. 2006.

[38] A. Ishimaru. *Wave Propagation and Scattering in Random Media*. Academic, New York, 1978.

[39] M. Karimi and M. Nasiri-Kenari. Ber analysis of cooperative systems in free-space optical networks. *Journal of Lightwave Technology*, 27(24):5639 –5647, dec.15, 2009.

[40] S. Karp and R. Gagliardi. The design of a pulse-position modulated optical communication system. *IEEE Transactions on Communication Technology*, 17(6):670 –676, december 1969.

[41] S. Karp, R. Gagliardi, S. E. Moran, and L. B. Stotts. *Optical Channels*. Plenum, New York, 1988.

[42] J. N. Laneman, D. N. C. Tse, and G. W. Wornell. Cooperative diversity in wireless networks: Efficient protocols and outage behavior. *IEEE Transactions on Information Theory*, 50(12):3062 – 3080, dec. 2004.

[43] E. J. Lee and V. W. S. Chan. Part 1: optical communication over the clear turbulent atmospheric channel using diversity. *IEEE Journal on Selected Areas in Communications*, 22(9):1896 – 1906, nov. 2004.

[44] N. Letzepis, K. Nguyen, A. Guillen i Fabregas, and W. Cowley. Outage analysis of the hybrid free-space optical and radio-frequency channel. *IEEE Journal on Selected Areas in Communications*, 27(9):1709 –1719, december 2009.

[45] J. Li and M. Uysal. Achievable information rate for outdoor free space optical communication with intensity modulation and direct detection. *Proc. IEEE Global Telecommunications Conference, 2003. GLOBECOM '03*, 5:2654–2658 vol.5, Dec. 2003.

[46] M. R. Luettgen, J. H. Shapiro, and D. M. Reilly. Non-line-of-sight single-scatter propagation model. *Proc. OSA*, A8:1964–1972, 1991.

[47] R.J. McIntyre. The distribution of gains in uniformly multiplying avalanche photodiodes: Theory. *IEEE Transactions on Electron Devices*, 19(6):703 – 713, jun 1972.

[48] F. Nadeem, V. Kvicera, M. S. Awan, E. Leitgeb, S. Muhammad, and G. Kandus. Weather effects on hybrid fso/rf communication link. *IEEE Journal on Selected Areas in Communications*, 27(9):1687 –1697, december 2009.

[49] S. M. Navidpour, M. Uysal, and M. Kavehrad. Ber performance of free-space optical transmission with spatial diversity. *IEEE Transactions on Wireless Communications*, 6(8):2813 –2819, august 2007.

[50] O. Oyman, N.J. Laneman, and S. Sandhu. Multihop relaying for broadband wireless mesh networks: From theory to practice. *IEEE Communications Magazine*, 45(11):116 –122, november 2007.

[51] G. Prati and R. Gagliardi. Block encoding and decoding for the optical ppm channel (corresp.). *IEEE Transactions on Information Theory*, 28(1):100 – 105, jan 1982.

[52] John G Proakis. *Digital Communications 3rd Ed.* McGraw Hill, New York, 1995.

[53] D. M. Reilly, D. T. Moriarty, and J. A. Maynard. Unique properties of solarblind ultraviolet communication systems for unattended ground sensor networks. *Proc. SPIE*, 5611:244–254, Oct. 2004.

[54] M. Safari and M. Uysal. Relay-assisted free-space optical communication. *IEEE Transactions on Wireless Communications*, 7(12):5441 –5449, december 2008.

[55] A. Sendonaris, E. Erkip, and B. Aazhang. User cooperation diversity. part i. system description. *IEEE Transactions on Communications*, 51(11):1927 – 1938, nov. 2003.

[56] A. Sendonaris, E. Erkip, and B. Aazhang. User cooperation diversity. part ii. implementation aspects and performance analysis. *IEEE Transactions on Communications*, 51(11):1939 – 1948, nov. 2003.

[57] M. Shatalov, J. Zhang, A. S. Chitnis, V. Adivarahan, J. Yang, G. Simin, and M. A. Khan. Deep ultraviolet light-emitting diodes using quaternary alingan multiple quantum wells. *IEEE J. Sel. Top. Quantum Electron.*, 8:302–309, 2002.

[58] G. A. Shaw, A. M. Siegel, and J. Model. Extending the range and performance of non-line-of-sight ultraviolet communication links. *Proc. SPIE*, 62310C:1–12, 2006.

[59] G. A. Shaw, A. M. Siegel, J. Model, and M. L. Nischan. Field testing and evaluation of a solar-blind uv communication link for unattended ground sensors. *Proc. SPIE*, 5417:250–261, 1991.

[60] G. A. Shaw, A. M. Siegel, and M. Nischan. Demonstration system and applications for compact wireless ultraviolet communications. *Proc. SPIE*, 5071:241–252, 2003.

[61] M. K. Simon and M. Alouini. *Digital Communication over Fading Channels: A Unified Approach to Performance Analysis*. Wileys, New York, 2000.

[62] D. Snyder. Filtering and detection for doubly stochastic poisson processes. *IEEE Transactions on Information Theory*, 18(1):91 – 102, jan 1972.

[63] T. A. Tsiftsis, H. G. Sandalidis, G. K. Karagiannidis, and N. C. Sagias. Multihop free-space optical communications over strong turbulence channels. In *IEEE International Conference on Communications, 2006. ICC '06.*, volume 6, pages 2755 –2759, june 2006.

[64] M. Uysal, S. M. Navidpour, and Jing Li. Error rate performance of coded free-space optical links over strong turbulence channels. *IEEE Communications Letters*, 8(10):635 – 637, oct. 2004.

[65] E. C. Van Der Meulen. Three-terminal communication channels. *Advances in Applied Probability*, 1(3):120 – 154, 1971.

[66] S Verdu. Poisson communiation theory. *The International Technion Communication Day in honor of Israel Bar-David*, Mar. 1999.

[67] L. Wang, Q. He, Z. Xu, and B. M. Sadler. Performance of non-line-of-sight ultraviolet communication receiver in isi channel. *Proc. SPIE*, 2010.

[68] S. G. Wilson. *Digital Modulation and Coding*. Prentice Hall, Upper Sadle River, New Jersy, 1996.

[69] S. G. Wilson, M. Brandt-Pearce, Q. Cao, and M. Baedke. Optical repetition mimo transmission with multipulse ppm. *IEEE Journal on Selected Areas in Communications*, 23(9):1901 – 1910, sept. 2005.

[70] J. M. Wozencraft and I. M. Jacobs. *Principles of Communication Engineering*. John Wiley and Sons, Inc., London, 1965.

[71] Z. Xu. Approximate performance analysis of wireless ultraviolet links. In *IEEE International Conference on Acoustics, Speech and Signal Processing, 2007. ICASSP 2007.*, volume 3, pages III–577 –III–580, april 2007.

[72] Z. Xu, G. Chen, F. Abou-Galala, and M. Leonardi. Experimental performance evaluation of non-line-of-sight ultraviolet communication systems. *Proc. SPIE*, 67090Y:1–12, 2007.

[73] Z. Xu, H. Ding, B. M. Sadler, and G. Chen. Analytical performance study of solar blind non-line-of-sight ultraviolet short-range communication links. *Opt. Lett.*, 33(16):1860–1862, 2008.

[74] Z. Xu and B.M. Sadler. Ultraviolet communications: Potential and state-of-the-art. *IEEE Communications Magazine*, 46(5):67–73, May 2008.

[75] X. Zhu and J. M. Kahn. Markov chain model in maximum-likelihood sequence detection for free-space optical communication through atmospheric turbulence channels. *IEEE Transactions on Communications*, 51(3):509 – 516, march 2003.

[76] X. Zhu and J. M. Kahn. Performance bounds for coded free-space optical communications through atmospheric turbulence channels. *IEEE Transactions on Communications*, 51(8):1233 – 1239, aug. 2003.

[77] Y. Zou, Zheng B., and Zhu J. Outage analysis of opportunistic cooperation over rayleigh fading channels. *IEEE Transactions on Wireless Communications*, 8(6):3077 –3085, june 2009.